Uniwersytet Śląski w Katowicach
Instytut Fizyki
Zakład Fizyki Teoretycznej

Andrzej Więckowski
Nr albumu: 292715

Dynamics of disordered quantum annealers

Praca magisterska

Promotor:
prof. zw. dr hab. Marcin Mierzejewski

Katowice 2018

Słowa kluczowe:
`adiabatic quantum computing`, `quantum annealing`, `graph coloring`,
`Ising model`, `D-Wave`

Oświadczenie autora pracy

Ja, niżej podpisany Andrzej Więckowski, autor pracy dyplomowej pt. *Dynamics of disordered quantum annealers*, o numerze albumu: 292715, student Wydziału Matematyki, Fizyki i Chemii Uniwersytetu Śląskiego w Katowicach, kierunku studiów Fizyka, specjalności *theoretical physics* oświadczam, że ww. praca dyplomowa:

- została przygotowana przeze mnie samodzielnie[1],

- nie narusza praw autorskich w rozumieniu ustawy z dnia 4 lutego 1994 r. o prawie autorskim i prawach pokrewnych (tekst jednolity Dz. U. z 2006 r. Nr 90, poz. 631, z późn. zm.) oraz dóbr osobistych chronionych prawem cywilnym,

- nie zawiera danych i informacji, które uzyskałem w sposób niedozwolony,

- nie była podstawą nadania dyplomu uczelni wyższej lub tytułu zawodowego ani mnie, ani innej osobie.

Oświadczam również, że treść pracy dyplomowej zamieszczonej przeze mnie w Archiwum Prac Dyplomowych jest identyczna z treścią zawartą w wydrukowanej wersji pracy.

Jestem świadomy odpowiedzialności karnej za złożenie fałszywego oświadczenia.

....
(miejsce i data)

....
(podpis autora pracy)

---

[1]uwzględniając merytoryczny wkład promotora (w ramach prowadzonego seminarium dyplomowego)

ii

To my parents Monika and Marek, beloved Karolina and everyone, who supported me during my education.

Thanks to Marcin Mierzejewski for being the best mentor and for guiding me on the right path.

iii

iv

Abstract

Quantum computers can be a big step for further advancement of our technology. The main focus of this work was to study disordered quantum annealing as an example method related to quantum computing. The first chapter introduces theoretical background of the thesis. The second one presents tests of numerics and comparison to Landau-Zener formula – a simple model of transitions in two level system. The last chapter, the most important one, presents an application of quantum annealing to specific combinatorial problem – graph coloring. We found out that a specific disorder can provide better results in quantum annealing than standard homogeneous system setting. Potentially, this method can be applied to D-Wave's quantum annealer to solve some problems more efficiently.

Streszczenie

Badania nad komputerami kwantowymi mogą stanowić duży postęp w dalszym rozwoju naszej technologii. Głównym celem tej pracy było badanie wyżarzania kwantowego z nieporządkiem, metodą związaną z obliczeniami kwantowymi. Pierwszy rozdział wprowadza czytelnika do podstaw teoretycznych związanych z tematem pracy. Drugi przedstawia testy numeryki i porównanie do formuły Landaua-Zenera – prosty model dwupoziomowego układu. Ostatni, najważniejszy, przedstawia zastosowanie wyżarzania kwantowego do wybranego problemu kombinatorycznego – kolorowania grafu. Pokazaliśmy, że odpowiedni nieporządek układu może zagwarantować lepszą wydajność wyżarzania kwantowego niż standardowe ustawienia. Potencjalnie ta metoda może zostać wykorzystana w kwantowym wyżarzaczu D-Wave do efektywniejszego rozwiązywania wybranych problemów.

Contents

viii

Introduction

Computers are probably the most important inventions in the history of mankind. They can be found in every aspects of our life. They can help us, support us or even they can save our lives. However, we are still trying to improve the performance of computers to do better and faster calculations with lower energy consumption.

In the last century, from about 60's until now, approximately every 2 years, total number of transistors in CPU has doubled. This statement is formulation of the famous *Moore's law* [1]. Nowadays, current advancement has slowly been decelerating and some people start to believe that in the about ~ 2020 Moore's law will not work anymore [2]. Greater miniaturization of integrated circuits slowly reaches the limit of quantum scales. Reaching this limit may cause some problems for future improvements of such technology. Our classical computation mostly depends on Boolean algebra with standard logic. In classical computers we wish to get rid of any quantum nature effects, to work on well defined classical bits: 0 and 1. Is it possible to construct such machine, which will benefit from quantum phenomena? If so, what are the advantages of quantum over classical computation. That is the questions which quantum computing is trying to find an answer for.

It is highly probable that we owe the early development (i.e. main idea) of quantum computing to these three scientists and their corresponding works: Paul Benioff [3], Yuri Manin [4] and Richard Feynman [5]. Then, some progress has been achieved. People developed algorithms for some problems, which had better performance than any other algorithm which could be performed on classical computers. Deterministic[2] Deutsch-Jozsa algorithm[6] allows to check if such binary function $f : \{0,1\}^n \to \{0,1\}$ is constant or balanced with only one evaluation. In classical algorithm, in worst case, $2^{n-1} + 1$ evaluations are needed. Probabilistic Grover algorithm[7] lets us search n-element database in $\mathcal{O}(\sqrt{n})$ steps, unlike classical algorithm $\mathcal{O}(n)$. Finally Shor's algorithm[8], probably most popular and most prominent algorithm, finds prime factors for given number in polynomial time (using quantum computer). On classical

---

[2] Most of quantum algorithms are probabilistic. A successful final results is obtained with huge probability. Deterministic ones mean that one has 100% probability of success (on reliable machine).

machine no one has ever found algorithm which works in polynomial time. The best known algorithm works in sub-exponential time. These algorithms made scientific community interested in the further development of the field. Especially the lastest algorithm which has been mentioned. Properly working quantum computer with efficient number of qubits should be able to crack current security cryptosystems which are in use today.

Considering computational complexity classes, quantum computers are perceived by many people as hope for finding an algorithm which can more effectively than any classical one solve some significantly difficult tasks. In Figure 1 a scheme of hypothetical[3] relationship between some important complexity classes of decision problems is presented. Decision problem is the one, which can be answered either by yes or no. Class **P** stands for *polynomial time* class, which means that this kind of problems can be solved efficiently in poly-
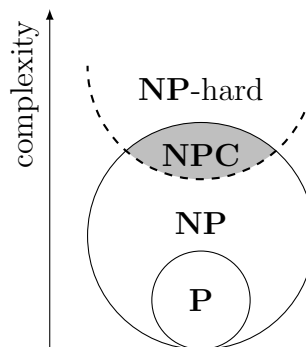

Figure 1: Hypothetical complexity relations between: **P**, **NP**, **NPC**, **NP**-hard classes.

nomial time on the deterministic machine. Class **NP** corresponds to *nondeterministic polynomial time* class, which includes problems for which solution can efficiently be validated in polynomial time. Class **NP**-hard includes *hard* problems. If all problems $A \in$ **NP** can be reduced in polynomial time to problem B, then problem B belongs to **NP**-hard. **NP**-hard can also include non-decision problems (e.g. *function problems* or *optimization problems*), for which there exist related decision problem. Class **NPC** stands for *nondeterministic polynomial complete* class and it is an intersection between **NP** and **NP**-hard. **NPC** includes the hardest problems from **NP**. Quantum computers could solve efficiently problems in **BQP** class[9] (with at least 2/3 probability). Acronym **BQP** represents bounded error quantum polynomial time. Relations between **BQP** and other listed classes still remain unknown. For example integer factorization problem is suspected to be outside **P** and should be in **BQP**, due to Shor's algorithm. However, we still do not now if an algorithm of integer factorization which works in polynomial time exists on classical machines. We do not know if problems efficiently solved by quantum machine can be also solvable efficiently on classical one, but nevertheless the algorithms listed above seem to be promising for quantum computing development.

---

[3] It is not certain if **P**≠**NP** or **P**=**NP**. Probably most of the scientist believe that **P**≠**NP**. This is one of the millennium problems.

What about physical realization? In the past few years, real race has begun. The adventure with actual experimental quantum computer began in 1998, when the first realization of Grover's algorithm was performed on 2 qubit system[10]. It was the beginning of the major progress. There are still some big challenges for the constructors. One of the biggest problems in the construction of such machines is quantum decoherence. After 20 years from the construction of the first 2-qubit system, technology has made some progress, but it is the beginning of even a greater story. The current status of the progress is the following: IBM company has 16-qubit universal quantum computer[11]; D-Wave Systems, first commercial quantum computer company, has in its offer 2048-qubit adiabatic quantum computers using quantum annealing[12]. The second company, at the beginning encountered a few problems. Scientific community did not believe that those machines are actual real quantum machines. Later studies proved that there is indeed a quantum entanglement phenomena on D-Wave's machines[13]. These two companies present two different approaches to quantum computing. Nowadays universal quantum computers have about ~ 10 qubits, while adiabatic quantum computers $\sim 10^3$ qubits and their total number grows according to Moore's law. Reaching the barrier of 10^6 qubits should bring huge perspective. In this work I will try to study the theoretical aspects of quantum computing such as D-Wave's machines.

What's inside?

The following thesis is divided into 3 chapters leading the reader from theoretical aspects to applications. The information included is supported by some derivations, formulas, pictures, schemes and some numerical results.

- In Chapter 1, a reader can find some basic definitions and topics related to adiabatic quantum computing: basic information about qubits, entanglement, quantum annealing and adiabatic theorem.

- In Chapter 2 there are some details of mathematical model, which can describe D-Wave machines. There are some tests of numerical methods and comparison to a simple two level system.

- Chapter 3 presents the results of adiabatic quantum computer application to solve graph coloring problems. It starts from mathematical background for graph theory and then there are some implementations of selected problems.

- In the appendixes the reader can find valuable materials regarding numerical methods or derivation of the Landau-Zener formula.

Chapter 1

Adiabatic quantum computing

1.1 Quantum computing

There are many models of quantum computing or even the classical ones (selected models are listed in Fig. 1.1). In this thesis we will focus on a very specific model, i.e. adiabatic model[14, 15]. Adiabatic quantum computing (AQC) model relies on the adiabatic theorem (see Section 1.5 for further details) and the calculations are based on this theorem. Other most 'popular' models are: circuit and topological models. The first model, the most 'popular', uses *quantum gates*[9, 16] to perform calculations as an analogy to classical bits register. The last one, probably the most subtle and prominent, uses braiding of *anyones*[17]. Due to better stability of this particles for decoherence, these kind of computation should be protected from small perturbations, which other models of quantum computing are not secured from.
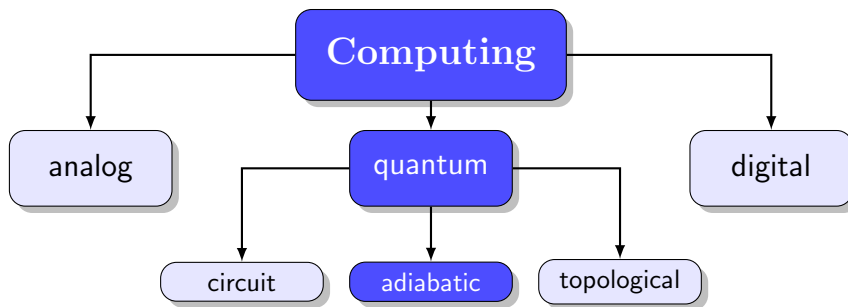
Figure 1.1: Selected classical and quantum computing models.

AQC is much different than others quantum computational models. Computation does not run in a specific sequence of gates or operations. Here calculations are based on initial/final Hamiltonian $\hat{H}_{i/f}(t)$ and a path from one to the other. As a results calculations are performed only by defining topology of the system described by Hamiltonian $\hat{H}_{i/f}(t)$, parameters of the Hamiltonian and their time dependence (see Section 1.6). However, this approach is polynomially equivalent to circuit gate model[18].

4

1.2 Qubits

Computers are usually defined as machines, which should be able to store, process and save information. Most of modern computers are based on binary system[1], in which we store informations using *bits* – the smallest amount of information. Bit can be represented by two distinguishable states 0, 1. The smallest amount of quantum information is a *qubit*. In a contrast to classical bits, qubits can be in any *superposition* of two quantum states: $|0\rangle$, $|1\rangle$ (Dirac *bra-ket* notation). These two vectors made up the base of two dimensional Hilbert space $\mathcal{H}(\mathbb{C}^2)$. In this space $\mathcal{H}$, any qubit can be represented by normalized vector $|\psi\rangle$:

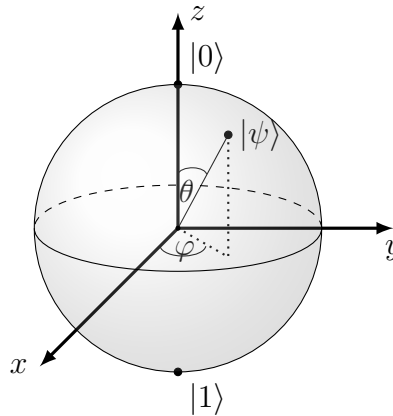$$|\psi\rangle = \alpha|0\rangle + \beta|1\rangle, \tag{1.1}$$

Figure 1.2: Bloch sphere: representation of the qubit.

where normalization condition holds: $|\alpha|^2 + |\beta|^2 = 1$ and α, β are complex parameters. Interpretation of parameters α, β is the following: when we do the measurement, $|\alpha|^2, |\beta|^2$ are the probabilities of outcome $|0\rangle, |1\rangle$ respectively. Since $\alpha, \beta \in \mathbb{C}$ one should expect that $|\psi\rangle$ can be described by 4 independent parameters. However $|\psi\rangle$ has only 2 degrees of freedom (not 4). One degree is absorbed by normalization condition and the other is neglected, because we have a free choice of phase $e^{i\omega}$. If one chooses $\alpha = e^{i\omega}\cos\frac{\theta}{2}$, then (it can be easily shown that) $\beta = e^{i\omega}e^{i\varphi}\sin\frac{\theta}{2}$, where $\omega, \theta, \varphi \in \mathbb{R}$. We end up with the following representation (we set $\omega = 0$):

$$|\psi\rangle = \cos(\tfrac{\theta}{2})|0\rangle + e^{i\varphi}\sin(\tfrac{\theta}{2})|1\rangle, \tag{1.2}$$

where θ, φ satisfy $0 \leqslant \theta \leqslant \pi$ and $0 \leqslant \varphi \leqslant 2\pi$. Any state from $\mathcal{H}$ can be described by this formula. The full range of parameters θ, φ defines famous

---

[1]Nowadays almost all of them are binary. However, in the early days of computing, in Soviet Union there were some computers using the balanced ternary numeral system (three-valued logic system) e.g. *Setun* [19].

Bloch sphere[9] (see Fig. 1.2).

In the real physical systems, qubits can be realized in many different ways. In Table 1.1 some selected realizations are presented. The reader can find information about various solutions using different particles and physical phenomena. There are many ideas, but still new ideas emerge. Most of the realizations are based on a two level system or a system in which we try to separate ground states and first excited states from the rest of the energy spectrum. A key role here is the temperature. Low temperature guarantees that the system should stay at the ground state and the first excited states as well as it ensures its protection from thermal noise.

Physical phenomena	Model	Information support	$\|0\rangle$ $\|1\rangle$
photon	polarization encoding	polarization	horizontal vertical
	number of photons	N	vacuum 1 particle
electrons	electronic spin	spin	up down
	number of electrons	N	vacuum 1 particle
Josephson junction	superconducting charge	island charge	uncharged charged
	superconducting flux	current	clockwise counterclockwise
	superconducting phase	energy state	ground state first excited state
Singly charged quantum dot pair	electron localization	charge (particle position)	left dot right dot

Table 1.1: Selected qubit implementations (source: wikipedia:Qubit). In D-Wave qubits were implemented with the method marked with a red contour.

D-Wave System's computers operate using Josephson junctions (see Section 1.4 for details). This method is marked in Table 1.1 by red dashed contour.

1.3 Entanglement

Except superposition of qubits, another very important phenomenon, which is missing in classical physics, can occur in quantum computer. It is called *entanglement*. Entanglement of particles can be defined as a state, in which particles can not be described independently anymore. From mathematical

6

perspective subsystems A and B are *not entangled* if they can be described by the following wave-function[2]:

$$|\Phi\rangle = |\psi\rangle_A \otimes |\phi\rangle_B \in \mathcal{H}_A \otimes \mathcal{H}_B. \qquad (1.3)$$

The measurement of physical quantities (eg. spin projection, photon polarization) of entangled objects has correlation which is absent in classical physics. For example, let us consider the following state $\frac{1}{\sqrt{2}}(|00\rangle + |11\rangle)$. In actual situation, 0,1 can be assigned to measured spin in z-axis in 2 entangled electrons. If we measure 0 on the first particle then we can be sure that if we measure the second particle (on the same basis) it will also be in state 0. Entanglement can be realized on very large distances and does not involve any retardation. It might seem that this phenomenon should lead to propagation of information at ∞ speed, but this is a paradox. In such experiment there is no validation of propagation limit at the speed of light c, because before the measurement we do not know in which state there are the particles, so no information propagation is done at all.

This strange non-local behavior was tested in experiments in the past few years by entanglement of different elementary particles (e.g. electrons[20], photons[21]) or even bigger objects like atoms[22] and molecules[23]. Most of these experiments are based on validation of the *Bell inequalities*. Entanglement has a very important role in quantum computing. Utilizing this phenomenon one can formulate fast working quantum algorithm, which overheads exponentially classical algorithms[9].

1.4   D-Wave hardware

Now we will focus on the example of quantum computers from real life, i.e. AQC or more precisely, the ones which rely on quantum annealing protocol. Within the past few years D-Wave System constructed several computers. Each new generation was better than the previous ones[12, 24, 25]. The first final product (not prototype) was a 128-qubit system. The newest computer has 2048 qubits. The company products can be described as analogous to Moore's law (Fig. 1.4). This is good news for us, because in a few years better performance in AQC will probably be achieved.

The newest machine, D-Wave 2000Q[12], is highly shielded from external magnetic field, and its quantum processing unit (QPU analogous CPU), the size of the thumb, is cooled down to extremely low temperature ~ 15 [mK].

---

[2] Definition can be expanded into mixed states ($p_i < 1$) using density matrices framework $\hat{\rho} = \sum_i p_i |\psi_i\rangle\langle\psi_i|$, where p_i is a probability that system is in state $|\psi_i\rangle\langle\psi_i|$. State $\hat{\rho}$ is entangled, if it cannot be represented in the following form: $\sum_i p_i \hat{\rho}_i^A \otimes \hat{\rho}_i^B$ and $\hat{\rho}_i^A \in \mathcal{H}_A$, $\hat{\rho}_i^B \in \mathcal{H}_B$.

(a) qubits in red
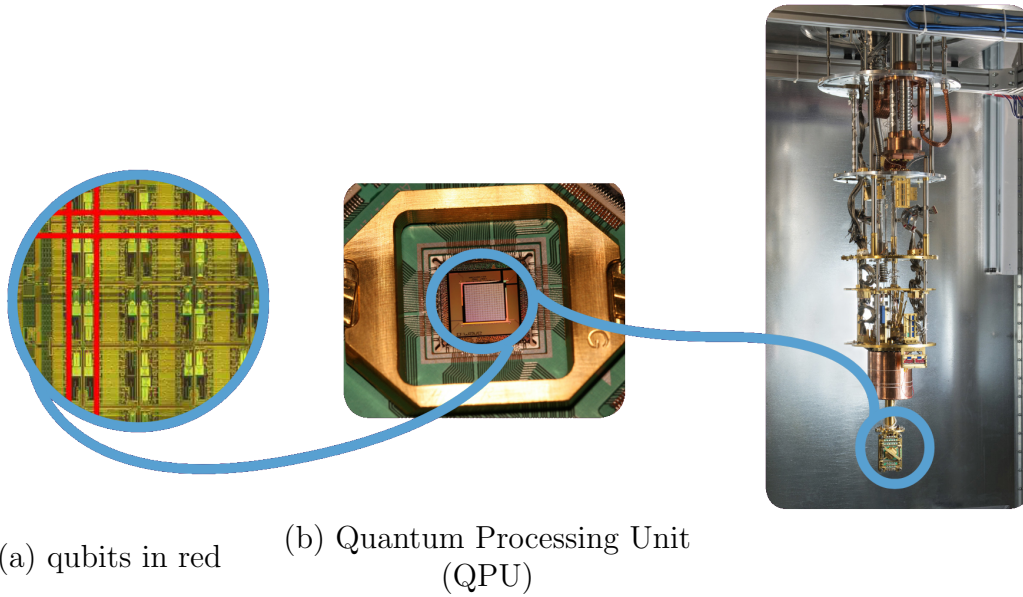
(b) Quantum Processing Unit (QPU)

Figure 1.3: Inside D-Wave's 'fridge' (Image source: [12]).

This low temperature guarantees that in D-Wave environment, some quantum effects, which are required for quantum computing, should appear while decoherence is suppressed. The whole construction has the following dimensions (approximately): length 3 [m], width 2 [m] and height 3[m].

As it was mentioned in Section 1.2, D-Wave qubits are based on Josephson junctions and they use superconducting flux and direction of the current. Single qubit, based on niobium[12], which is a superconductor below temperature 9.2[K], is built by two superconducting loops [26] (see Fig 1.5). Such a system can be modelled by two-well potential in which potential U barrier is proportional to flux Φ_2, and potential extrema heights difference h is related to flux Φ_1. In that system there can be current flows clockwise – this state can be assigned to $|0\rangle$, counterclockwise – this can be assigned to $|1\rangle$ or in both directions – this can be assigned to a superposition $|\psi\rangle = \alpha|0\rangle + \beta|1\rangle$.
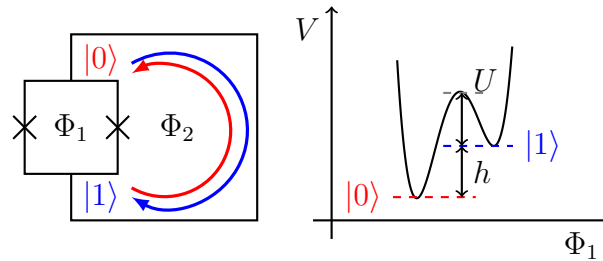

Figure 1.5: Simplified flux qubit scheme with corresponding modeled potential $V(\Phi_1)$. Colored arrows in diagram represent corresponding current flow direction. Cross symbol 'X' in the circuit means a Josephson junction.
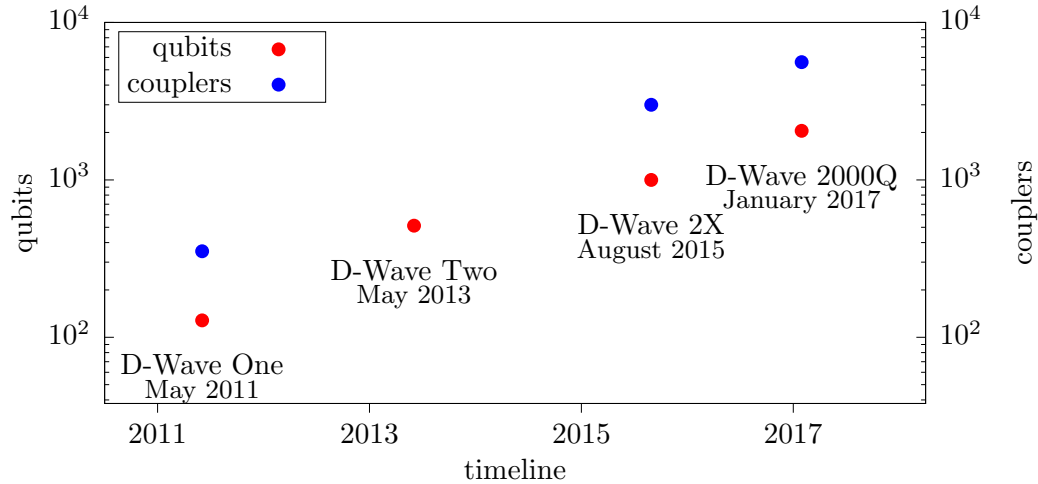
8

Figure 1.4: D-Wave's analogue of the Moore law.

Qubits in D-Wave machines are connected via chimera topology. A part of complicated connections (couplers) structure is presented in Figure 1.6. The grid for D-Wave 2000Q contains 256 units (colored with blue), each containing 8 qubits, which can be divided into two groups of 4 qubits: vertical and horizontal ones. Each unit of qubits forms *bigraph*. Each qubit from one group is connected to all qubits from the other group and it is not connected to any qubit from its group. Units are connected in such a way that vertical/horizontal qubits are connected with neighboring vertical/horizontal qubits (colored with red). Since our system is a finite system, some of the units have only 2 or 3 neighbors (not 4). These units are certainly located on the grid edge (color gray). Since not all connections between qubits are available, one should properly embed studying case into such topology, if our qubits resource is sufficient.
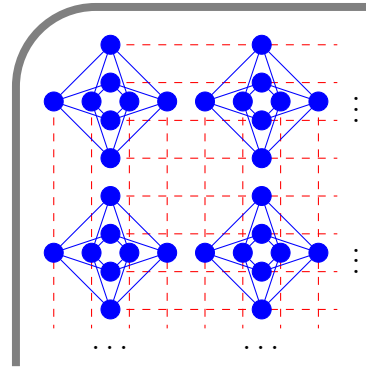

Figure 1.6: Chimera graph topology realized on D-Wave machines.

1.5 Adiabatic theorem

AQC relies on very important theorem: *adiabatic theorem*. This theorem holds that if a system is in n-eigenstate (especially ground state) of initial Hamiltonian $\hat{H}_i$ and then a system is evolved adiabatically in time (slowly

enough) to final Hamiltonian $\hat{H}_{\mathrm{f}}$, then the system will remain in n-eigenstate[3]. The first proof of this theorem was given by Fock and Born[27] in 1928. The following section will be devoted to proving this theorem (derivation is based on a book [28]).

In general, evolution of the quantum state $|\psi\rangle \in \mathcal{H}$ of the system, which can be described with Hamiltonian $\hat{H}$, is given by equation of motion – *time-dependent Schrödinger equation* (TDSE) [28]:

$$i\hbar|\dot{\psi}\rangle = \hat{H}|\psi\rangle, \tag{1.4}$$

where the dot means a derivative with respect to time t, $\hbar$ is Planck constant. To make it more convenient, all other formulas, calculation or numerics in this thesis are done with units $\hbar = 1$. In the case of time independent Hamiltonians, Equation (1.4) may be solved by finding eigenstates of $\hat{H}$ [*time-independent Schrödinger equation* (TISE)]:

$$\hat{H}|n\rangle = E_n|n\rangle, \tag{1.5}$$

where $|n\rangle$ are stationary solutions to Schrödinger equation and they obey orthonormal relations $\langle m|n\rangle = \delta_{nm}$, so they can be used as a base of the Hilbert space $|\psi\rangle = \sum_n c_n|n\rangle$. Putting Eq. (1.5) into Eq. (1.4) with condition $|\psi\rangle = |n\rangle$ one can obtain that for time independent Hamiltonian the solution of Schrödinger equation is as follows:

$$|n(t)\rangle = |n(0)\rangle \exp\left(-i\int_0^t \mathrm{d}t' E_n\right) = |n(0)\rangle \exp\left(-iE_n t\right). \tag{1.6}$$

During the evolution, $|n\rangle$ only picks up a phase factor, which can be eliminated by some gauge transformation and it is irrelevant during measurement.

However, eigenproblem can be solved for time-dependent Hamiltonian:

$$\hat{H}(t)|n(t)\rangle = E_n(t)|n(t)\rangle \tag{1.7}$$

and even now eigenstates obey orthogonal relations: $\langle m(t)|n(t)\rangle = \delta_{nm}$. One can write general solution $|\psi\rangle$ for Equation (1.4) using eigenstates $|n(t)\rangle$:

$$|\psi(t)\rangle = \sum_n c_n(t)|n(t)\rangle e^{i\theta_n(t)}, \tag{1.8}$$

where θ_n is a *dynamical phase*:

$$\theta_n(t) = -\int_0^t \mathrm{d}t' \, E_n(t'). \tag{1.9}$$

---

[3] Assuming discrete, non-degenerate spectrum through all evolution from $\hat{H}_{\mathrm{i}}$ to $\hat{H}_{\mathrm{f}}$.

Introducing dynamical phase is only a convention. Such phase could be inserted into definition: $c_n \rightarrow c_n e^{i\theta_n}$. Choice of θ_n is motivated by solution for time independent Hamiltonian like in Equation (1.6). The next step is to put $|\psi\rangle$ into Schrödinger equation:

$$\begin{cases} i|\dot{\psi}\rangle = \hat{H}|\psi\rangle; \\ i|\dot{\psi}\rangle = i\sum_n \Big(\dot{c}_n|n\rangle + c_n|\dot{n}\rangle + c_n|n\rangle i\dot{\theta}_n\Big)e^{i\theta_n}; \\ \hat{H}|\psi\rangle = \sum_n c_n\hat{H}|n\rangle e^{i\theta_n} = \sum_n c_n E_n|n\rangle e^{i\theta_n}. \end{cases}$$

After some algebraic calculations one can end up with the following equation:

$$i\sum_n \Big(\dot{c}_n|n\rangle + c_n|\dot{n}\rangle\Big)e^{i\theta_n} = 0. \tag{1.10}$$

Next, Equation (1.10) is multiplied from the left hand side by $\langle m|e^{-i\theta_m}$:

$$\sum_n \Big(\dot{c}_n\langle m|n\rangle + c_n\langle m|\dot{n}\rangle\Big)e^{i(\theta_n-\theta_m)} = 0;$$

$$\sum_n \Big(\dot{c}_n\delta_{mn} + c_n\langle m|\dot{n}\rangle\Big)e^{i(\theta_n-\theta_m)} = 0;$$

$$\dot{c}_m = -\sum_n c_n\langle m|\dot{n}\rangle e^{i(\theta_n-\theta_m)}. \tag{1.11}$$

Now the only missing element is $\langle m|\dot{n}\rangle$. It can be obtained from differentiating Equation (1.7):

$$\dot{\hat{H}}|n\rangle + \hat{H}|\dot{n}\rangle = \dot{E}_n|n\rangle + E_n|\dot{n}\rangle.$$

After that, the equation is multiplied from the left hand side by arbitrary eigenstate $\langle m|$:

$$\langle m|\dot{\hat{H}}|n\rangle + \langle m|\hat{H}|\dot{n}\rangle = \dot{E}_n\langle m|n\rangle + E_n\langle m|\dot{n}\rangle;$$

$$\langle m|\dot{\hat{H}}|n\rangle + E_m\langle m|\dot{n}\rangle = \dot{E}_n\delta_{mn} + E_n\langle m|\dot{n}\rangle;$$

$$\langle m|\dot{n}\rangle = \frac{\langle m|\dot{\hat{H}}|n\rangle - \dot{E}_n\delta_{mn}}{E_n - E_m}.$$

The last step is to put $\langle m|\dot{n}\rangle$ into Equation (1.11) and factor out from summation the element where $n = m$:

$$\dot{c}_m = -c_m\langle m|\dot{m}\rangle - \sum_{n\neq m} c_n\frac{\langle m|\dot{\hat{H}}|n\rangle}{E_n - E_m}e^{i(\theta_m-\theta_n)}.$$

In the adiabatic regime one can approximate $\dot{H} \approx 0$ and the last term will drop out:

$$\dot{c}_m \approx -c_m \langle m|\dot{m}\rangle. \tag{1.12}$$

As a result, a first order differential equation is achieved and the next step is to separate the variables and integrate it:

$$\int_0^t \mathrm{d}t' \, \frac{\dot{c}_m}{c_m} = -\int_0^t \mathrm{d}t' \, \langle m|\dot{m}\rangle;$$

$$c_m(t) = c_m(0)\exp\left(-\int_0^t \mathrm{d}t' \, \langle m|\dot{m}\rangle\right). \tag{1.13}$$

Now the geometric phase $\gamma_m(t)$ will be introduced:

$$\gamma_m = i\int_0^t \mathrm{d}t' \, \langle m|\dot{m}\rangle;$$

$$c_m = c_m(0)e^{i\gamma_m}.$$

The value of $\langle m|\dot{m}\rangle$ is purely imaginary. From orthogonality relation of eigenvectors $\langle m|n\rangle = \delta_{nm}$ one gets:

$$\langle m|m\rangle = 1;$$

$$\langle \dot{m}|m\rangle + \langle m|\dot{m}\rangle = 0;$$

$$(\langle m|\dot{m}\rangle)^* + \langle m|\dot{m}\rangle = 0 \rightarrow \Re(\langle m|\dot{m}\rangle) = 0.$$

Finally, the solution of Schrödinger equation is obtained in adiabatic approximation [Eq. (1.12)]. After the evolution state $|\psi\rangle$ only picks up some phases:

$$|\psi(t)\rangle = \sum_n c_n(0)|n(t)\rangle e^{i\theta_n(t)}e^{i\gamma_n(t)}. \tag{1.14}$$

1.6   Quantum annealing

In the literature one can notice that terminologies: AQC and *Quantum annealing* (QA) are used interchangeably. Nevertheless, one should be careful and distinguish these concepts, because they are slightly different. However, using AQC and QA alternately should not lead to misunderstandings.

AQC is a computational model [14, 15], which is able to solve any problem which universal quantum computer (gate model) should be able to solve (with maximally some polynomial time penalty)[18]. The main idea of AQC is based
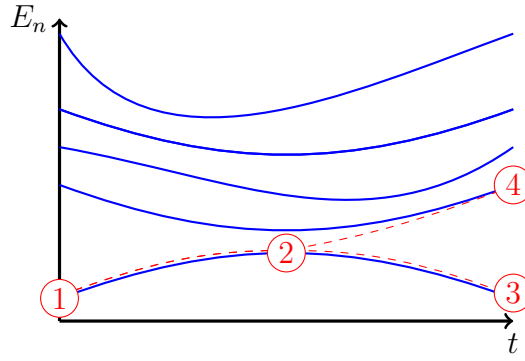
Figure 1.7: Energy spectrum E_n in a function of time t for arbitrary Hamiltonian.

on the adiabatic theorem. First, initial state is started from easy initial Hamiltonian $\hat{H}_i$ ground state. Then the system is evolved on some path associated with function $f(\tau) \in [0,1]$, $f(-1) = 1$, $f(1) = 0$, $\tau \in [-1,1]$, into ground state, due to adiabatic theorem, of a final, desired Hamiltonian $\hat{H}_f$, which is constructed in such a way that it should produce the correct answer included in a ground state for a specific problem. It is worth mentioning that, since adiabatic theorem holds not only for a ground state, but for the all eigenstates of Hamiltonian, one should be able also to carry out the computing with excited states. However, probably this solution will be harder to establish, because of difficulties in designing such Hamiltonian and manipulation with adiabatic evolution. Time dependent Hamiltonian of system $\hat{H}(\tau = t/T)$ can be written in the following form:

$$\hat{H}(\tau) = f(\tau)\hat{H}_i + [1 - f(\tau)]\hat{H}_f.$$

It can be shown that runtime T (total evolution time) of an algorithm in such a language of AQC will produce correct answer with enough probability, which should be rounded with[29]:

$$T = \mathcal{O}\left(\frac{1}{\min(\text{gap})^2}\right),$$

where $\mathcal{O}$ is a *big o notation* and a $\min(\text{gap})$ is minimal energy gap between ground state energy and first excited state energy in Hamiltonian spectrum in the hole range of time. When T is not large enough, then the adiabatic theorem stops working and we get higher and higher probability that the system will end in some excited state with not necessarily correct answer which we hope to obtain from the final state. Here in Figure 1.7, we have a simplified picture presenting some energy spectrum in a function of time for arbitrary Hamiltonian:

① initial state of Hamiltonian as a ground state;

13

② here at midpoint, where the gap is minimal, this point is the most significant, the gap determines the probability that the system will remain in its ground state;

③ success, the correct answer is obtained – if we are lucky or if the gap was large enough to neglect probabilities of a transition to excited state;

④ we end up with an excited state – the gap was too small (or misfortune) and the correct answer is not obtained.

QA is a *heuristic* method for solving optimization combinatorial problems[15]. Most of these tasks belongs to **NP**-hard complexity class. Alternatively QA can be considered as a physical (or simulated) realizations of some algorithms from AQC. QA owes its name to *simulated annealing* (SA). In some way it is a precursor of QA. Simulated annealing is a technique for global optimization of some function – e.g. finding minimum. Inspiration of this method was annealing (heat treatment) in metallurgy. The principle of operation of

Figure 1.8: Schematic view on the difference between mechanism of SA and QA.

this technique is very similar to *Monte Carlo* methods or *Metropolis algorithm*. The algorithm starts from a random state of the problem. Next, one tries to alter the state slightly. Then, some quantity of current state is measured and the decision if new modified state is accepted or not is made with some probability (depending on temperature). In the next steps of the algorithm, the temperature is decreased to sufficiently low limit. With some probability at each step there is a chance that the state will become worse than in the previous iteration. This is very important and purposeful because it prevents from stacking in some local minima. It can be compared to thermal fluctuations, which should be able to move the system in potential landscape in the direction of global minima (Figure 1.8). In the contrast to thermal fluctuation in SA, quantum fluctuations are used in QA. The algorithm starts from generating all possible states of the system with equal probability. Then the system evolves in time due to Schrödinger equation. During evolution *transverse field*[4] is being changed (parameter plays similar role as temperature in SA). This parameter changes enable the system to tunnel in a potential landscape as a results of changing the amplitudes of all possible states. If evolution is being performed slowly enough, then correct answer will be obtained with large probability. In
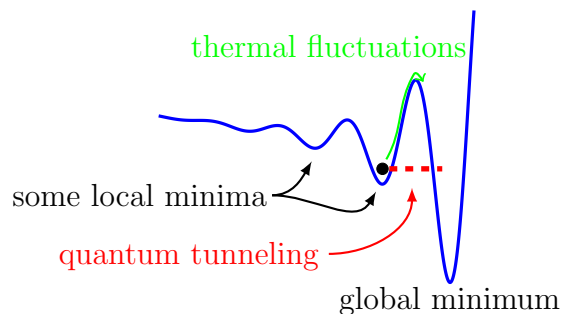
---

[4]It will be explained in the next Chapter 2.

Figure 1.8 the difference between physical phenomena behind SA and QA is sketched. In the contrast to a general AQC, QA has some restrictions:

- initial state should be a superposition of all possible states in the system with non-zero probability, e.g.: $|\psi\rangle = \frac{1}{2^L} \sum_{i=0}^{2^L-1} |\text{bin}(i)\rangle$ (L is number of qubits);

- final Hamiltonian $\hat{H}_f$, should be the classical one, as mostly solved problems are the combinatorial ones – for example *Ising model* for describing spin glass.

Chapter 2

Ising model with transverse field

In this chapter the first results will be presented, together with considering a very simple model, i.e. Ising chain[30] with an additional term. First, the studied model will be described and some details of the annealing procedure will be explained. The purpose of this part of the thesis is to test the numerics and demonstrate the physical phenomena related to (a)diabatic evolution.

2.1   Hamiltonian

D-Wave's machines can be considered as a physical realization of the Ising model[15, 26]. The model can be described as generalized Ising model with a transverse field [31]as given by the Hamiltonian $\hat{H}$:

$$\hat{H}(\tau) = -A(\tau)\left(\sum_{i=1}^{L}\Delta_i\sigma_i^x\right) - B(\tau)\left(\sum_{\langle i,j\rangle}J_{ij}\sigma_i^z\sigma_j^z + \sum_{i=1}^{L}h_i\sigma_i^z\right),\qquad(2.1)$$

where σ_i^x, σ_i^z are Pauli spin operators, e.g. $\sigma_i^z = 2s_i^z$; J_{ij} is interaction between 2-components of spins on site i and j; h_i is a value of an external magnetic field (direction z) coupled to spin on site i; Δ_i is a value of a transverse field (direction x) and $A(t)$, $B(t)$ are linear time-dependent functions, whose behaviors are visualized on Figure (2.1). However, on actual D-Wave machines $A(\tau), B(\tau)$ are slightly different [32], but the approximation presented in Figure 2.1 is sufficient. As $A(\tau)$ is changed in time, at the end of evolution only the second term of Hamiltonian, which is classical, remains. This is a requirement on QA as it was mentioned in Section 1.6. At the beginning evolution starts only with the first term of Hamiltonian (2.1). The initial state is a ground state for $\hat{H}(-1)$, which may be obtained from *Lanczos algorithm*[1] (see Appendix A.1 for details). Schrödinger Equation (1.4) is solved for appropriate

---

[1] However, the state can be received analytically very easily in x and then transformed into z basis, but for work convenience the system is described in z basis and it is replaced with the general algorithm. This step does not affect the performance substantially and allows one to study case with disordered Δ_i as well.
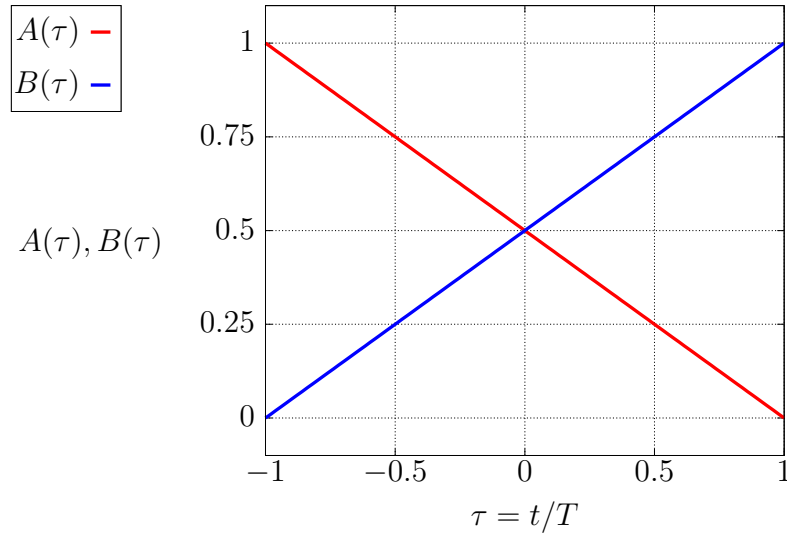
Figure 2.1: Behaviors of functions $A(\tau)$, $B(\tau)$.

time-dependent protocol for functions $A(\tau), B(\tau)$. The evolution is obtained by the expansion of propagator operator in a *Chebyshev polynomial* basis (see Appendix A.2 for details) with sufficiently small time step $\delta t = 0.01$, even for huge fields h_i. At the end, the final state is achieved, in which one can measure some observables as well as some quantities during evolution.
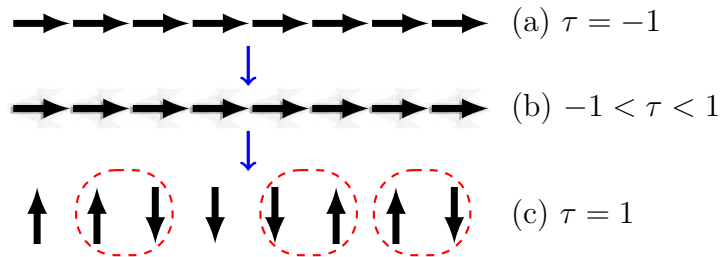
2.2 Test of implementation

Figure 2.2: Sketch of evolution: (a) initial state – fully polarized state; (b) state changes during evolution – superposition and tunneling of amplitudes take place; (c) final state – ferromagnetic state with defects depending on annealing time – marked with red dashed circles.

As a test, a simple uniform chain [described by Hamiltonian (2.1)] is studied, with $L = 20$, $\Delta_i = 2$, $J_{ij} = 1$, $h_i = 0$ and with open boundary conditions (OBC). The topology of the chain is the following: $\langle i, j \rangle \rightarrow \langle i, i+1 \rangle$ for $i = 1, \dots, L-1$. In this section $B(\tau) = B = 1$ is fixed only temporarily, as was done in [33]. In this paper [33], authors calculated kinks (defects) which emerge
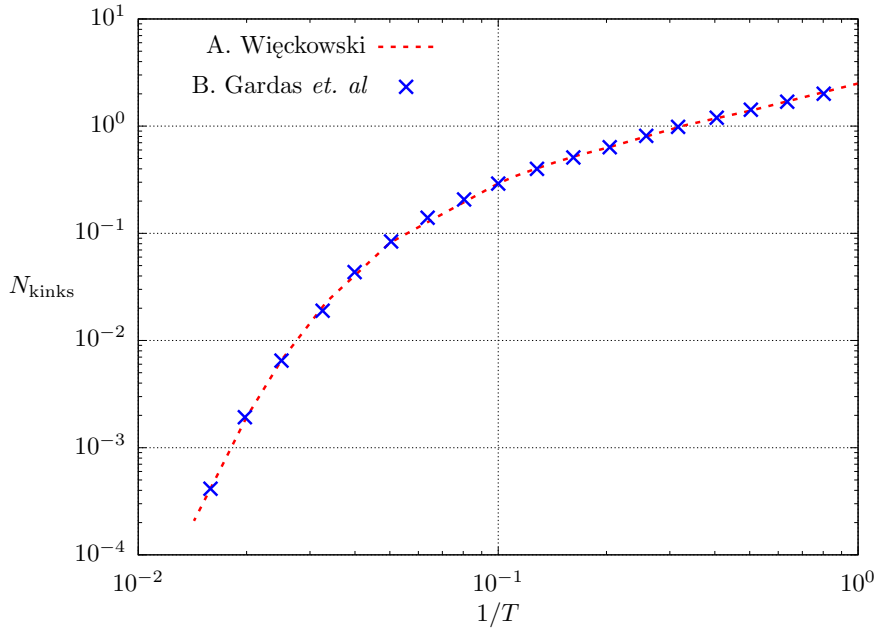
Figure 2.3: Code test – comparison between my results (red) and results from the paper [33] (blue). Number of kinks N_{kinks} as a function of inverse time T (system size $L = 20$, $\Delta_i = 2$, $h_i = 0$, $J_{ij} = 1$, $B(\tau) = B = 1$, chain, OBC). Note: double log scale.

after annealing. The ground state of $\hat{H}(-1)$ i.e. the initial state is in the form: $|\rightarrow\rightarrow \cdots \rightarrow\rangle$ – spins are fully polarized in x-direction. The ground state of final Hamiltonian $\hat{H}(1)$ is degenerate: $|\uparrow\uparrow \ldots \uparrow\rangle$ and $|\downarrow\downarrow \ldots \downarrow\rangle$. Depending on evolution time T, different number of kinks (defects) should appear in the system. Kinks can be defined as a number of neighbouring spins with opposite directions e.g. state $|\uparrow\uparrow\uparrow\downarrow\downarrow\rangle$ has 1 kink. The sketch of evolution procedure is shown in Figure 2.2. Kinks can be calculated from final state by using the following quantity:

$$N_{\text{kinks}} = \frac{1}{2} \sum_{\langle i,j \rangle} \left(1 - \langle \sigma_i^z \sigma_j^z \rangle \right). \tag{2.2}$$

To explain origin of this quantity, the following example will be considered: $|\uparrow\uparrow\uparrow\downarrow\downarrow\rangle$ (it has 1 kink). The first, second and the last pair of spins have zero contribution to the sum. Only the third pair gives the contribution equal 2, so a proper counting factor $\frac{1}{2}$ should be taken into account before summation. The main purpose of defining such observable is to confront the results with the published ones [33]. Results in [33] have been obtained for $h_i = 0$, when the system can be mapped on non-interacting fermions. In Figure 2.3 there is the comparison of the results. As one can see the results are in the perfect agreement, despite using different methods to obtain them.

One should be aware that in general kinks in quantum computers defined as in Equation (2.2) do not quantify excitations. For inhomogeneous systems, spins do not need to be fully polarized. However, in the present case the ground state is fully polarized and Equation (2.2) quantifies density of excitations.

2.3 Results

In this section, an extended model from the previous section will be studied, with non-zero external field $h_i \neq 0$ and our model will be compared to analytic results for just two level system: the Landau-Zener formula (LZF). It is recommended to follow LZF derivation and numerical results from Appendix B. All restrictions from previous section (like freezing the function $B(t)$) are relaxed as well.

2.3.1 Testing energy level spectrum
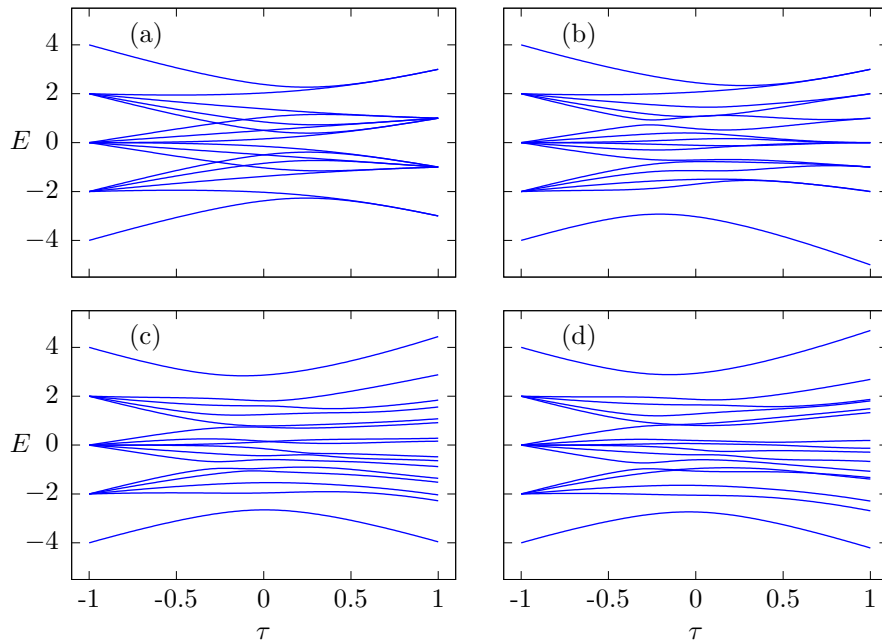
Figure 2.4: Energy spectrum for Hamiltonian (2.1) for different cases (selected ones): (a) $J_{ij} = 1$, $h_i = 0$, (b) $J_{ij} = 1$, $h_i = 0.5$, (c) $J_{ij} = 1$, $h_i = \text{rand}(1)$ (d) $J_{ij} = 1 + \text{rand}(0.25)$, $h_i = \text{rand}(1)$, where $\text{rand}(a)$ is a uniform random distribution from $-a$ to a. (chain with $L = 4$, OBC, $\Delta_i = 1$).

First, energy spectrum during the whole evolution for short chains ($L = 4$) is studied [by solving TISE (1.5)]. Even in such a small system, there are $2^4 = 16$ eigenstates, but energy spectrum is degenerate (for uniform, ideal chain) has only up to 5 or 4 distinct eigenvalues. Initial/final system has significant

degeneracy in the whole spectrum. However, this degeneracy can be decreased by adding constant field h_i or fully destroyed by introducing some disorder in J_{ij} or h_i. In Figure 2.4 an example of energy spectrum as a function of time for different cases is presented. In Figure 2.4a a result for uniform chain without any disorder and any field h_i is posted. For this case, energy spectrum is symmetric with respect to $E = 0$. The situation in Figure 2.4b is the most favorable case for adiabatic evolution. Here the gap between ground state and first excited state is the largest. However, still the final Hamiltonian has highly degenerate energy spectrum (7 distinct eigenvalues). Only if one introduces disorder in J_{ij} and h_i it will lift degeneracy of the final spectrum as shown in Figures 2.4c-d. One may draw conclusion that uniform field h_i should guarantee stability of QA, but one should also remember that here a model of a very simple problem is considered with trivial ground state like: $| \uparrow\uparrow \ldots \uparrow \rangle$. In general, our inputs are: topology of the lattice $\langle i, j \rangle$ and specific values of parameters J_{ij}, h_i. Depending on these inputs, after QA one should be able to obtain (any) ground state, e.g.: $| \uparrow\uparrow\downarrow\uparrow\downarrow\downarrow \ldots \rangle$.

2.3.2 Testing adiabaticity

As it was pointed out in Section 1.6, calculations are preformed according to the adiabatic theorem. The crucial question is how slowly the evolution should be performed to achieve the correct answer with large probability. In Figure 2.5 a schematic look into this problem is presented. If evolution is performed too fast then the system should end up (with huge probability) in an excited state, probably returning wrong answer to the problem. Verification of adiabacity condition can be tested, by calculating energy difference of the final state: $\langle \hat{H} \rangle$ and ground state energy of the final Hamiltonian: E_0. Such a test will be presented in the next two Figures: 2.6, 2.7.

Figure 2.6 illustrates how such energy difference changes during evolution process. The energy E_0 is the ground-state energy of Hamiltonian at time t and it is calculated by Lanczos Algorithm (see Appendix A.1). Evolutions
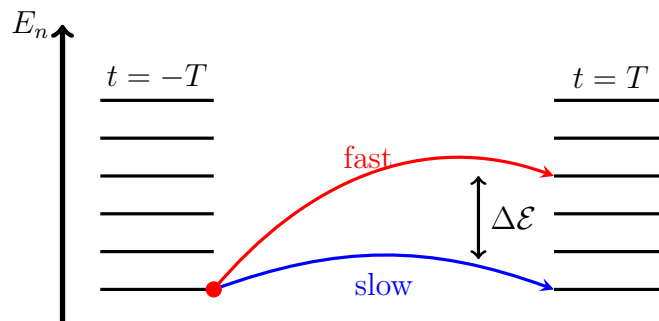

Figure 2.5: Schematic dependence of evolution speed and energy excitation.

were carried out using Chebyshev polynomials (see Appendix A.2) with same settings as in Section 2.1. Initial state $|\psi\rangle$ was calculated by solving TISE for Hamiltonian (2.1) at $\tau = -1$. Evolutions realized in total time T are marked with corresponding colors. As it can be noticed, this quantity gets smaller exponentially with increasing T, which is verified in the next Figure 2.7. In Figure 2.7, shows the energy difference at the end of evolution as a function of T. As one can see, energy difference indeed decreases exponentially when T grows.
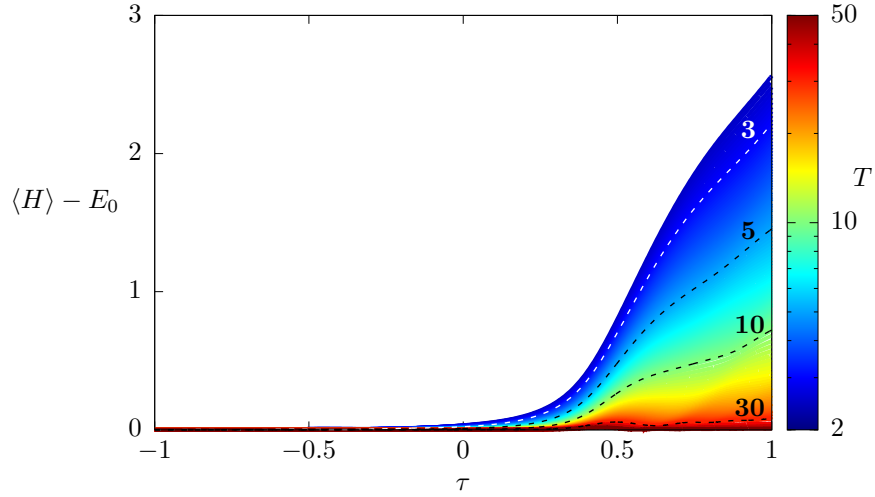
Figure 2.6: Energy difference $\langle \hat{H} \rangle - E_0$ as a function of evolution normalized time τ. Evolutions with total time T are marked with colors. Selected paths for corresponding T are marked with dashed lines, ended with labels. ($L = 12$, $J_{ij} = 1$, $h_{ij} = 0$, $\Delta_i = 2$, OBC)
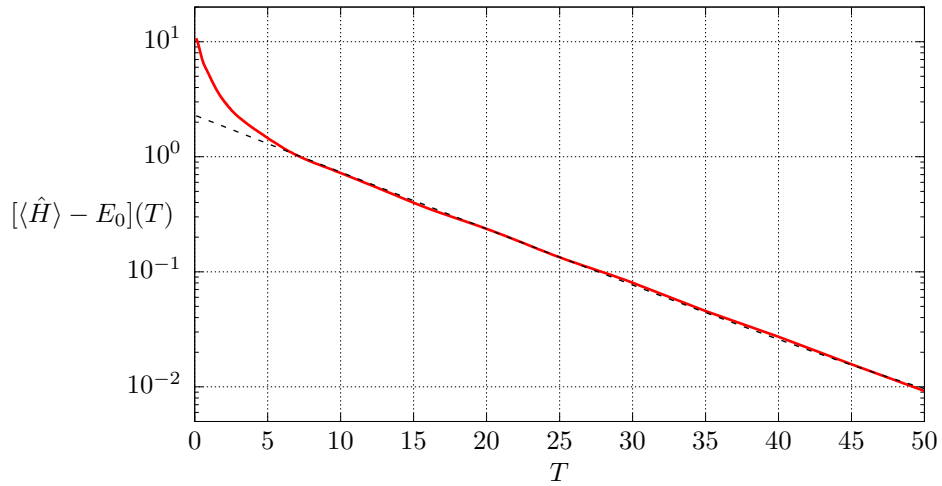
Figure 2.7: Solid red line: energy difference $\langle \hat{H} \rangle - E_0$ as a function of evolution time T. Black dashed line corresponds to fitted exponential function in the range $T \in [5, 50]$. ($L = 12$, $J_{ij} = 1$, $h_{ij} = 0$, $\Delta_i = 2$, OBC)

21

We can use this energy difference solely to test how much evolution is adiabatic. In the next Section 2.3.3 another, more useful method is proposed.

2.3.3   Comparison to Landau-Zener formula

In this section the results for other quantity will be presented, which can be used to estimate annealing time T that is sufficient for adiabatic evolution. Instead of calculating kinks in the system or energy difference from state and ground state, one can simply calculate projection of state to ground state of final Hamiltonian. This quantity $|\langle\psi_0|\psi\rangle|^2$ contains information about probability that our state $|\psi\rangle$, obtained from Schrödinger equation (TDSE), is the ground state $|\psi_0\rangle$ of final Hamiltonian (2.1) at $\tau = 1$. Here, the same numerical methods and their setting were applied as in Section 2.1. Figure 2.8a shows projection F_0 as a function of T for a system with uniform h_i:

$$F_0 = |\langle\psi_0|\psi\rangle|^2. \tag{2.3}$$

As one can see even small value of constant field h_i, can rapidly increase the probability of success.

Except for studying the probability, we try to compare our system to the dynamics of a simple two level system, described by Hamiltonian:

$$\hat{H}_{LZ} = \frac{1}{2}\alpha t\sigma_z + \frac{1}{2}\beta\sigma_x. \tag{2.4}$$

Such a system can be studied exactly. The transition probability is given by the Landau-Zener formula discussed in Appendix B. From Equation (B.15), probability of a transition is given by: $\mathcal{P}_{LZ} = \exp(-\frac{\pi\beta^2}{2\alpha})$, so it is related to β and the slope α. However, we are interested in the opposite event – the system should remain in its ground state, so such probability can be expressed by:

$$\widetilde{\mathcal{P}}_{LZ} = 1 - \mathcal{P}_{LZ} = 1 - \exp(-\tfrac{\pi\beta^2}{2\alpha}). \tag{2.5}$$

The parameters α and β can be obtained by fitting the energy spectrum. Gap ΔE for LZF can be expressed by subtracting two eigenvalues from the Equation (B.2):

$$\Delta E = \sqrt{(\alpha\tau)^2 + \beta^2}.$$

In our case, we use this expression to fit the difference between the two lowest eigenenergies obtained from numerics. Here the minimum of gap is not always at $\tau = 0$ and the gap does not have symmetric shape. As a results, another parameter τ_0 must be added to the expression for gap. It is simply the position of the gap:

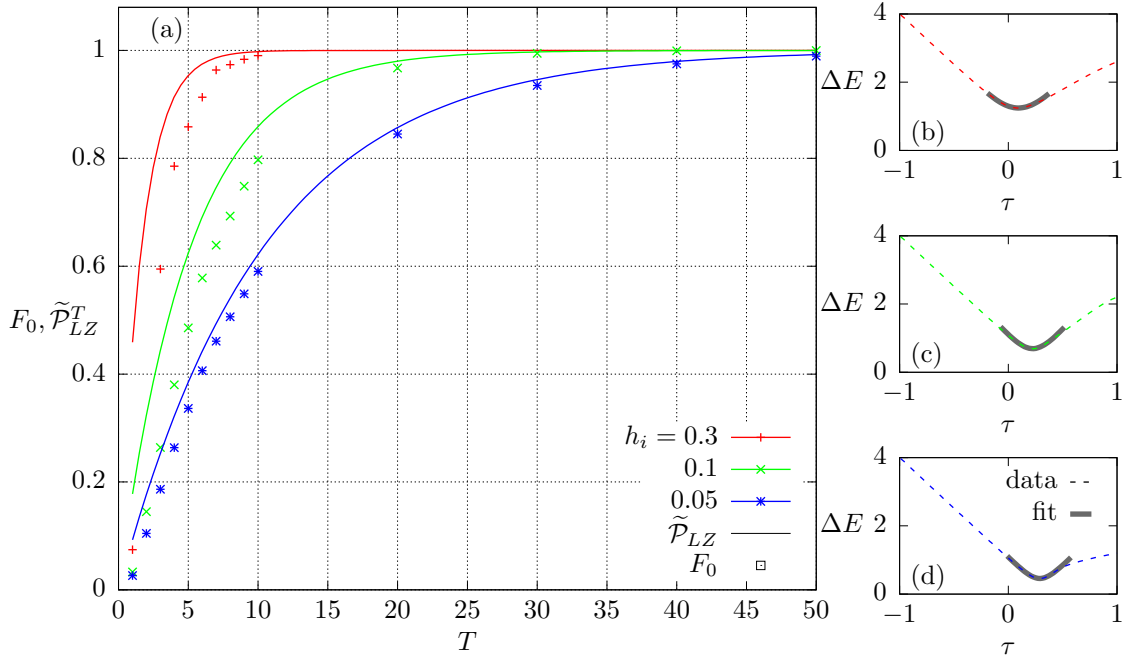$$\Delta E = \sqrt{[\alpha(\tau - \tau_0)]^2 + \beta^2}. \tag{2.6}$$

Figure 2.8: Comparison of numerical results with Landau-Zener formula: (a) numerically obtained projections F_0 [Eq. (2.3)] for systems with different uniform h_i are marked with points, the probability $\widetilde{\mathcal{P}}_{LZ}^{T}$ [Eq. (2.7)] obtained from LZF with fitted gap shown as a solid line; (b), (c), (d) numerical results (dashed line) fitted by Eq. (2.6) (gray bold line). Colors in (a) match colors in (b), (c), (d). ($L = 12$, $J_{ij} = 1$, $\Delta_i = 2$, OBC)

Since LZF was derived for infinite time range $t \in [-\infty, \infty]$, one should introduce proper scaling of Equation (2.5) to finite time range $t \in [-T, T]$ by rescaling $\alpha \rightarrow \frac{\alpha}{T}$:

$$\widetilde{\mathcal{P}}_{LZ}^{T} = 1 - \exp(-\tfrac{\pi \beta^2}{2\alpha} T). \tag{2.7}$$

In Figures 2.8b-d gaps for our studied system are presented. A fitted formula (2.6) is marked with a gray bold line. The fitting has to be carried out in a limited range of energies as close as possible to its minimum because of the lack of symmetry. In Figure 2.8a solid lines show probabilities of remaining in a ground state from the Landau-Zener formula with fitted parameters α, β from a gap. As it can be observed, results from LZF and actual data do not differ very much. Knowing the gap structure, LZF can give efficient estimation for proper annealing time T.

23

Chapter 3

Graph coloring in Ising model

3.1 Selected topics of graph theory

In this section, basics concepts and definitions from graph theory[34–36] will be introduced. Despite that graphs are kind of abstract object, they can be very useful for solving many everyday life problems. In many branches of physics, graph theory finds application, for example in Quantum Field Theory [37], Solid State Physics, Quantum Information Theory [38] or even in Astrophysics [39].

3.1.1 Definitions

First, definition of a graph is required. In this work, only specific cases of graphs are discussed: undirected graphs. Moreover, only connected graphs will be considered, i.e. graphs in which there exists a path from each vertex to any other vertex:

> **Definition 3.1.1: Undirected graph**
>
> *Undirected graph* $G(V, E)$ is an object containing: set of *vertices* V and multi-set of *edges* E. Multi-set E contains *unordered* pairs of vertices: $E = \{\{v, u\} : \{v, u\} \in V\}$. For simplicity elements from E will be written as (v, u).

Example 3.1.1.

Consider graph $G(V, E)$, where $V = \{1, 2, 3, 4\}$ and $E = \{(1, 1), (1, 2), (2, 3), (2, 3), (1, 3), (3, 4)\}$. This graph is shown in Figure (3.1).

In Fig. 3.1 vertices are represented by blue circles with labels, and edges are represented by red lines. As one can see, self-loops and repeated edges are allowed.
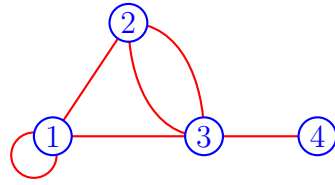
Figure 3.1: Pictorial representation of the graph from Example (3.1.1).

Definition 3.1.2: Simple graph

Simple graph is an undirected graph without self-loops and repeated edges. Self loops (v, v) and repeated edges $E = \{\ldots, (v_1, v_2), (v_1, v_2), \ldots\}$ are not allowed anymore.

If some edges from the previous Example 3.1.1 are reduced, then one can achieve graph which will satisfy simple graph conditions.
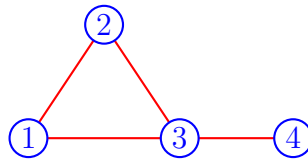
Figure 3.2: The modified graph from Figure 3.1 to satisfy simple graph conditions.

Definition 3.1.3: Complete graph

Complete graph K_n is an undirected simple graph, in which all pairs of vertices are connected by edges, where $n = |V|$.

(a) graph K_4 (b) graph K_5
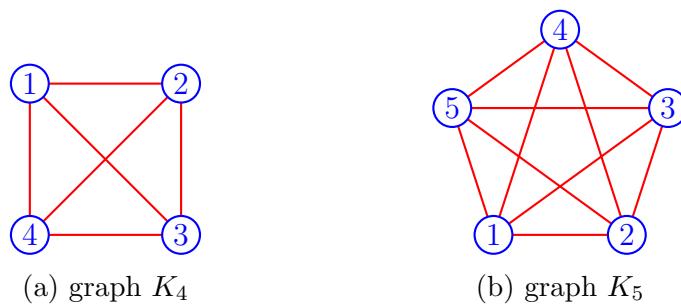
Figure 3.3: Complete graph examples.

Definition 3.1.4: Planar graph

Planar graph P is an undirected simple graph, which can be drawn in the plane in such a way that no edges cross each other.

In Figure 3.4 an example of planar graphs and non-planar graphs is demonstrated. In Figure 3.3a edge (1,3) can be removed outside the "box" to show that K_4 is indeed planar. From the graph in Figure 3.3b edges cannot be drawn in such a way that they do not cross each other – Figure 3.4b. However, this problem can be solved after extending the definition of the planarity condition. If one considers drawing not only in the plane, but in any other topological surface of a given *genus*[1] g, one can easily prove that for $g = 1$ (i.e. torus) even K_5 is planar.

(a) planar graph K_4 (b) non-planar graph (K_5)
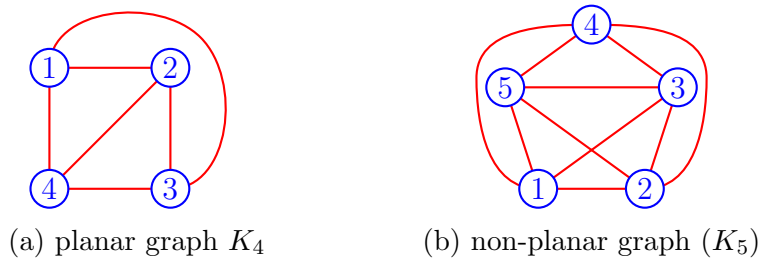
Figure 3.4: Example planar and non-planar graphs.

Planar graphs are very important graphs considering the case which will be introduced in later section. As it was shown before, for $|V| \leqslant 4$ all graphs are planar, but when $|V| \geqslant 5$ more and more graphs can not be classified as planar. In Figure 3.5 a relation between number of vertices and number of all non-isomorphic planar and simple graphs is presented. Non-isomorphism means that no bijection between two graphs exists, transforming one into the other. One can easily obtain data from Figure 3.5 using open source programs: `geng` and `plantri`.
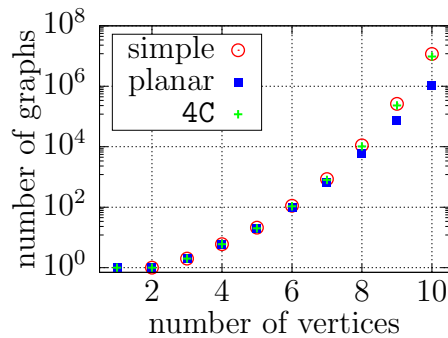
Figure 3.5: The number of non-isomorphic graphs versus the number of vertices for: simple, planar and 4-or-less-color $4C = \{G : \chi(G) \leqslant 4\}$ graphs.

3.1.2 Graph coloring

Graph coloring is a procedure in which, some labels (it can be color, number, sign, anything) are assigned to the graph's vertices or edges. This work is focused only on coloring of vertices. The task is to color graph in such a way, that non adjacent vertices will have common color. Often question is to find a *chromatic number* $\chi(G)$ of a specific graph G:

---

[1] *Genus* is a topological property – a number of holes in the manifold [40].

> **Definition 3.1.5: Chromatic number**
>
> *Chromatic number* $\chi(G)$ is a minimal number of colors, which are required to color graph G, in such a way that no two adjacent vertices share the same color.
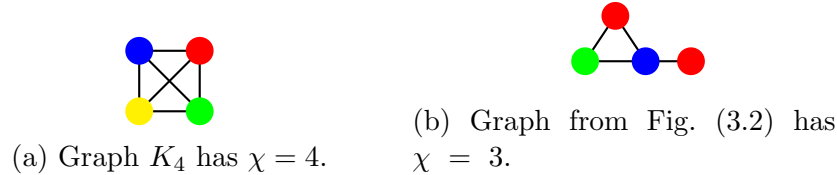

(a) Graph K_4 has $\chi = 4$.   (b) Graph from Fig. (3.2) has $\chi = 3$.

Figure 3.6: Example of graph coloring with its chromatic numbers.

One can easily prove that for all complete graphs K_n, the value of $\chi(K_n) = n$. There are some other rules for specific types of graphs, which can be found in Ref. [35]. In Figure 3.6 examples of graph coloring are shown. It should be pointed out that coloring procedure is not unequivocal. Graph in Figure 3.6a can be colored in $4! = 24$ different ways with the same set of colors: red, green, blue and yellow. By all means, using actual real colors will be useful only for graphs, which have small χ. For graphs with large value of χ it is better to use numbers to color it up. For any graph G, finding its $\chi(G)$ is a very difficult task. This problem can be assigned to **NP**-hard problems. Checking if graph G can be colored with k colors (without minimum criteria) is a **NPC** problem. Finally, counting possible solutions of coloring with k colors is located in **#P** problem class. **#P** includes counting problems related to corresponding decision problems from **NP**. However, for planar graphs, mathematicians have proved a very important theorem:

> **Theorem 3.1.1: Four-color theorem**
>
> For any planar graph P, chromatic number $\chi(P) \leqslant 4$. In general case, this theorem depend on how planarity is defined. For an oriented surface with given genus g this theorem holds[34]: $\chi(P) \leqslant \left\lfloor \frac{7+\sqrt{1+48g}}{2} \right\rfloor$.

This theorem was introduced without any explanation or proof, because for now exist only proofs with computer support[35]. Since any map (like in cartography) can be brought to a planar graph, main conclusion is that 4 color is enough for colorizing any map. In practice, cartographers are using more than 4 colors, for example in order to distinguish oceans and other water territories from countries or to mark coherent territorial country (e.g. Russia and Kaliningrad – Russian exclave). However, converse theorem does not exist, here is an example of a graph which has $\chi \leqslant 4$ and is not planar:
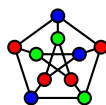
3.2 Mapping to Ising model

After a brief introduction to the graph theory, coloring problem implementation in a language of binary variables (or spins) will be discussed. One can find some other algorithms[41] (**NP** class), which can be implemented on the so-called QUBO formula. They can be easily mapped to the Ising model. This approach is a big perspective for future perfecting AQC, since D-Wave's machines are physical realization of such a model.

3.2.1 QUBO formula

Quadratic unconstrained binary optimization (QUBO) is a method [42], which can be used for solving selected **NP** class problems. The method is based on the minimizing the binary quadratic polynomial. The simplest formula can be examined as the following:

$$H = \sum_{i=1}^{N} c_i X_i + \sum_{i=1}^{N} \sum_{j=1}^{N} Q_{ij} X_i X_j, \tag{3.1}$$

where X_i is a binary variable $X_i \in \{0, 1\}$; c_i, Q_{ij} are real parameters $c_i, Q_{ij} \in \mathbb{R}$ and N is the total number of variables X_i. It is very similar to the Ising model. The only difference is that in the Ising model variables are not binary, they are spin variables S_i^z. Indeed one can find mapping from one to the other very easily. In this way, many problems can be implemented. The main idea is to find configuration of X_i variables, such that it will be give the minimum of H. During this procedure parameters c_i and Q_{ij} are given as inputs, and as a result not only the configuration with the minimum of H is carried out, but the value of $\min(H)$ as well.

A	B	C	H
0	0	0	0
0	0	1	0
0	1	0	1
1	0	0	−1
0	1	1	0
1	0	1	−2
0	1	1	1
1	1	1	−1

Table 3.1: All possible configuration for Figure 3.7.
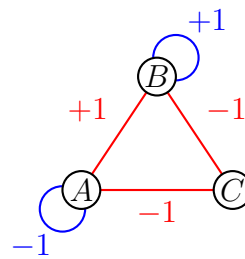
Figure 3.7: QUBO example.

Example 3.2.1.

For a better understanding example from Figure (3.7) is discussed. Values of c_i are represented as blue self-loops with the corresponding numbers and

the values of Q_{ij} are marked in red. If some connection (edge) is missing, it means that appropriate parameter is equal to 0. With n vertices the system always has 2^n possible configurations. For the case in Fig. 3.7, there are 8 possible configuration. In Table 3.1 all cases with the corresponding H are written down. The solution, configuration with the smallest value of H, is marked with red rectangle.

3.2.2 Graph coloring in QUBO formula

To properly define graph coloring problem in QUBO, one should introduce a binary variable X_{ic}, which is 1 if vertex $i \in \{1, 2, \dots n\}$ is colored with color $c \in \{1, 2, \dots, k\}$ and 0 if not. The first index enumerates vertices and the second one colors. One should enforce very important condition: each vertex i should be colored with one specific color c. This condition can be written in the following way:

$$\sum_{c=1}^{k} X_{ic} = 1. \tag{3.2}$$

This condition guarantees choosing exactly one color to each vertex. With this statement one should easily figure out how to embed a graph coloring [41]:

$$\hat{H}_G = \sum_{i=1}^{n} \underbrace{\left(1 - \sum_{c=1}^{k} X_{ic}\right)^2}_{H_{V_i}} + \sum_{\langle i,j \rangle} \underbrace{\sum_{c=1}^{k} X_{ic} X_{jc}}_{H_{E_{ij}}}. \tag{3.3}$$

Here $\langle i, j \rangle$ denotes summation over connected vertices. Term H_{V_i} provides penalty for each time when vertex is colored with more than one color or with no color at all. The second term, $H_{E_{ij}}$, generates penalty when connected vertices have the same color. The main stated problem is to find whether k colors allow for a proper coloring of a given graph G. When ground state with corresponding eigenenergy $E = 0$ exists, then graph G can be colored with k colors. The procedure ends not only with the

Figure 3.8: Schematic representation coloring problem of graph G in QUBO formula.

information about possibility of coloring, additionally properly colored graph is produced. One only needs to check which color of variables X_{ic} for specific vertex i gets value 1. In this problem the total number of required binary variables X_{ic} is equal to kn. In a sense, graph G is copied k times, each copy for one color. Each vertex is represented by k variables, each for one color as in
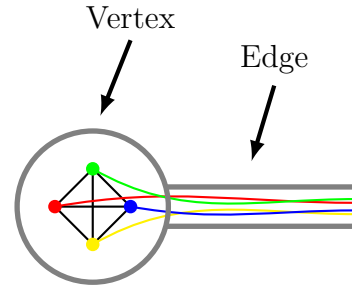
Figure 3.8.

Now this problem will be mapped to the Ising model. The only thing which should one do, is to transform all binary variables X_{ic} into spins S_{ic}. Since $X_{ic} \in \{0, 1\}$ and $S_{ic} \in \{-\frac{1}{2}, \frac{1}{2}\}$ one could transform it in the following way:
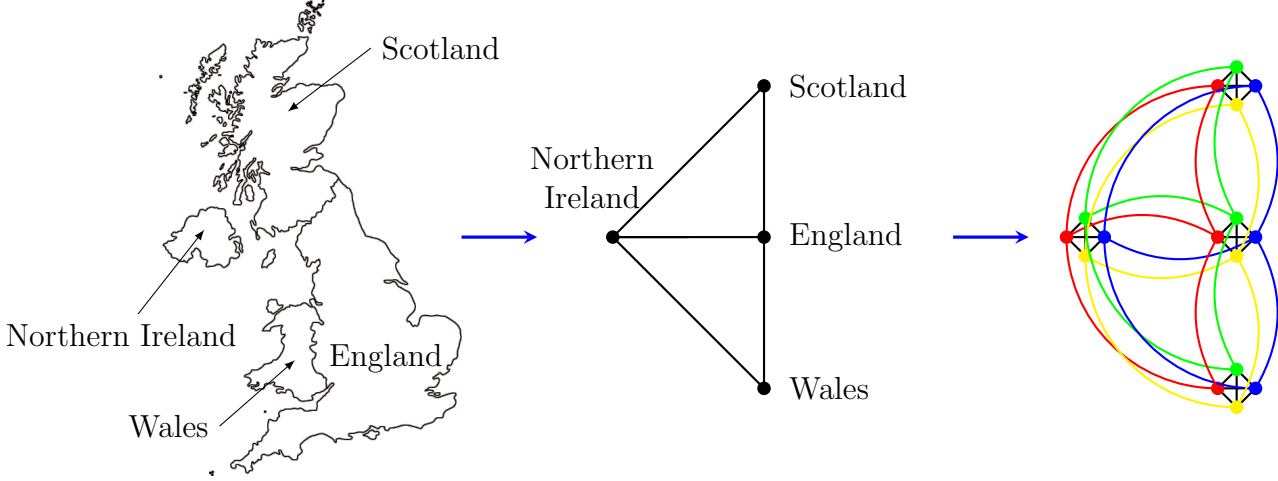

Figure 3.9: Schematic mapping *map coloring* problem into graph representation and next into equivalent the Ising formulation. (United Kingdom contour source: [43])

$$X_{ic} = S_{ic} + \frac{1}{2}. \tag{3.4}$$

One can starts from term H_{V_i} in Equation (3.3):

$$H_{V_i} = \left(1 - \sum_{c=1}^{k} X_{ic}\right)^2 = \left(1 - \sum_{c_1=1}^{k} X_{ic_1}\right)\left(1 - \sum_{c_2=1}^{k} X_{ic_2}\right) = 1 - \sum_{c_1=1}^{k} X_{ic_1} - \sum_{c_2=1}^{k} X_{ic_2} + \sum_{c_1=1}^{k} X_{ic_1} \sum_{c_2=1}^{k} X_{ic_2} =$$

$$= 1 - 2\sum_{c=1}^{k} X_{ic} + \sum_{c_1=1}^{k}\sum_{c_2=1}^{k} X_{ic_1}X_{ic_2} = 1 - 2\sum_{c=1}^{k} X_{ic} + \sum_{c_1=c_2} X_{ic_1}X_{ic_2} + \sum_{c_1 \neq c_2} X_{ic_1}X_{ic_2} =$$

$$= 1 - 2\sum_{c=1}^{k} X_{ic} + \sum_{c=1}^{k} \underbrace{X_{ic}^2}_{X_{ic}} + \sum_{c_1 \neq c_2} X_{ic_1}X_{ic_2} = 1 - \sum_{c=1}^{k} X_{ic} + 2\sum_{c_1 < c_2} X_{ic_1}X_{ic_2} =$$

$$= 1 - \sum_{c=1}^{k}\left(S_{ic} + \frac{1}{2}\right) + 2\sum_{c_1 < c_2}\left(S_{ic_1} + \frac{1}{2}\right)\left(S_{ic_2} + \frac{1}{2}\right) = 1 - \sum_{c=1}^{k} S_{ic} - \frac{k}{2} + 2\sum_{c_1 < c_2}\left(S_{ic_1} + \frac{1}{2}\right)\left(S_{ic_2} + \frac{1}{2}\right) =$$

$$= 1 - \sum_{c=1}^{k} S_{ic} - \frac{k}{2} + 2\sum_{c_1 < c_2} S_{ic_1}S_{ic_2} + \underbrace{\sum_{c_1 < c_2}(S_{ic_1} + S_{ic_2})}_{(k-1)\sum_c S_{ic}} + \frac{1}{2}\underbrace{\sum_{c_1 < c_2} 1}_{\frac{k(k-1)}{2}} = 1 + \frac{k(k-3)}{4} + (k-2)\sum_{c=1}^{k} S_{ic} + 2\sum_{c_1 < c_2} S_{ic_1}S_{ic_2}.$$

Now, the second term will be considered:

30

$$\sum_{\langle i,j\rangle} H_{E_{ij}} = \sum_{\langle i,j\rangle}\sum_{c=1}^{k} X_{ic}X_{jc} = \sum_{\langle i,j\rangle}\sum_{c=1}^{k}\left(S_{ic}+\frac{1}{2}\right)\left(S_{jc}+\frac{1}{2}\right) = \sum_{\langle i,j\rangle}\sum_{c=1}^{k} S_{ic}S_{jc} + \frac{1}{2}\sum_{\langle i,j\rangle}\sum_{c=1}^{k}(S_{ic}+S_{jc}) + \frac{1}{4}\sum_{\langle i,j\rangle}\sum_{c=1}^{k} 1 =$$

$$= \sum_{\langle i,j\rangle}\sum_{c=1}^{k} S_{ic}S_{jc} + \frac{1}{2}\sum_{i=1}^{n}\deg(i)\sum_{c=1}^{k} S_{ic} + \frac{1}{4}k|E|,$$

where $\deg(i)$ is a degree of vertex i, i.e. the number of edges that enter the vertex, $|E|$ is total number of edges of the problem graph G. Summarizing, problem from Equation (3.3) can be written in the spin language as following:

$$\hat{H}_G = \sum_{i=1}^{n}\left(1 + \frac{k(k-3)}{4} + (k-2)\sum_{c=1}^{k} S_{ic} + 2\sum_{c_1<c_2} S_{ic_1}S_{ic_2}\right) + \sum_{\langle i,j\rangle}\sum_{c=1}^{k} S_{ic}S_{jc} + \sum_{i=1}^{n}\deg(i)\sum_{c=1}^{k} S_{ic} + \frac{1}{4}k|E| =$$

$$= \left(1+\tfrac{k}{4}(k-3)\right)n + \frac{1}{4}k|E| + \sum_{i=1}^{n}\underbrace{\left(k+\tfrac{1}{2}\deg(i)-2\right)}_{\tilde{h}_i}\sum_{c=1}^{k} S_{ic} + 2\sum_{i=1}^{n}\sum_{c_1<c_2} S_{ic_1}S_{ic_2} + \sum_{\langle i,j\rangle}\sum_{c=1}^{k} S_{ic}S_{jc}.$$

$$(3.5)$$

In Figure 3.9 there is a schematic overview considering mapping: map coloring $\rightarrow$ graph coloring $\rightarrow$ Ising network. In this example coloring of United Kingdom's map is taken into account (assuming that Northern Ireland should has different color than other 3 Kingdoms). This graph is 3-chromatic[2] , provided that 3 colors are enough to color this graph. In this picture there are 4 colors visible in the Ising representation, nevertheless this is only schematic plot, showing that each vertex of graph G contains k nodes, in which every node is connected to all the others. It is worth mentioning that case when $k = 2$ is not interesting at all. One can use Ising model for anti-ferromagnet to solve 2-chromatic graph using only n qubits not nk.

3.3 Results

3.3.1 Studied topologies

All possible non-isomorphic topologies of graphs $G(E,V)$ with $n = |V|$ up for $n = 3, 4, 5$, which are k-chromatic (for $k > 2$), were studied. As a part of calculations, annealing was simulated by such protocol:

$$\hat{H}(\tau) = -A(\tau)\sum_{i=1}^{L=nk}\Delta_i\sigma_i^x + B(\tau)\hat{H}_G, \qquad (3.6)$$

where $\hat{H}_G$ is a Hamiltonian of coloring problem from Equation (3.5), $S_{ic} \rightarrow S_{ic}^z$ and $A(\tau), B(\tau)$ are functions discussed in Chapter 2. Technical details of the

---

[2]k-chromatic means that graph G has chromatic number $\chi(G) = k$.

evolution was described in Section 2.1. Coloring of a graph is unambiguous and then many solutions to this problem exist. This has an important consequence: almost all Hamiltonians from (3.5) for any graphs have huge degeneracy (see Table 3.2 for an overview of studied topologies). For each case unique `ID` is assigned: $\text{ID}(k, n, \mathfrak{t})$, where $k = \chi(G)$, $n = |V|$ and $\mathfrak{t}$ enumerates various topologies for graph $G(E, V)$ for fixed k and n. Unlike in the Chapter 2, simple projection F_0 [Eq. (2.3)] is not sufficient since there is huge degeneracy of the ground state in the system. The following projection F is proposed to be measured at the end of annealing, i.e. at time T:

$$F = \langle\psi(T)| \left(\sum_{i \in \mathbf{gs}} |i\rangle\langle i| \right) |\psi(T)\rangle = \sum_{i \in \mathbf{gs}} |\langle\psi(T)|i\rangle|^2. \qquad (3.7)$$

Here **gs** is a set of all ground states for a specific disorder-free problem encoded in Hamiltonian (3.5) and $|\psi(T)\rangle$ is a state obtained at the end of evolution (TDSE) for studied system with annealing protocol (3.6). Since one can write identity operator in following way: $\mathbb{1} = \sum_{i \in \mathbf{gs}} |i\rangle\langle i| + \sum_{i \notin \mathbf{gs}} |i\rangle\langle i|$, this projection is a very good method for measuring efficiency of reaching the ground state in the annealing time T. In Figure 3.10 we show projections as a function of T for all studied topologies. Increasing problem size (L) unnecessarily increase required time for the annealing. For each case `ID` is visible at a plot key.

Except calculations for pure systems, system with disorder was also examined. Such setup should simulate the situation, when actual values of interaction strengths differ from results obtained from maping QUBO on the Ising problem. The disorder was implemented by modification of specific terms in the Hamiltonian:

$$\text{disorder } h_i: \quad h_i S_i^z \rightarrow (h_i + \Delta h_i) S_i^z, \qquad \Delta h_i \in [-W_h, W_h];$$
$$\text{disorder } J_{ij}: \quad J_{ij} S_i^z S_j^z \rightarrow (J_{ij} + \Delta J_{ij}) S_i^z S_j^z, \quad \Delta J_{ij} \in [-W_J, W_J];$$

where here h_i, J_{ij} are corresponding values from H_{V_i} and $H_{E_{ij}}$ respectively, before adding disorder. Δh_i, ΔJ_{ij} are random variables with flat distributions with amplitudes W_h, W_J. In Figure 3.11 we show 100 realizations as a function of T for different values of the disorder amplitude W_h. Increasing W_h, increase spread out of the results. For case with huge value of $W_h = 1.0$ some of the realizations are much better then results without any disorder (note: double log scale), still there are some realizations that are not good at all. In Figures 3.12 and 3.13 there are repeated data from Figure 3.10 with additional lines corresponding to average results with disorder (h_i). All subplots are titled with graphs `ID` and one can see graph representation of studied topology on each subplot. Average disorder realizations make all cases worse, nevertheless there are indeed some realizations with disorder, when a better result then without noise was obtained. Calculation time grows exponentially with the system size L. Accordingly, for last cases with `ID`$(4, 4, 1)$, `ID`$(4, 5, 1)$, `ID`$(4, 5, 2)$ and

ID$(4, 5, 3)$ there are only results without disorder. However, introducing disorder to the system causes lack of information about number of solutions. Only one solution is favorable by the system, due to lifting degeneracy.

ID	k	n	$\mathtt{t}$	$|E|$	degeneracy	$\min\deg(i)$	$\max\deg(i)$	topology
ID$(3, 3, 1)$	3	3	1	3	6	2	2	
ID$(3, 4, 1)$	3	4	1	4	12	1	3	
ID$(3, 4, 2)$			2	5	6	2	3	
ID$(3, 5, 1)$	3	5	1	5	24	1	4	
ID$(3, 5, 2)$			2	5	24	1	3	
ID$(3, 5, 3)$			3	6	12	1	4	
ID$(3, 5, 4)$			4	7	6	2	4	
ID$(3, 5, 5)$			5	5	24	1	3	
ID$(3, 5, 6)$			6	6	12	2	4	
ID$(3, 5, 7)$			7	6	12	1	3	
ID$(3, 5, 8)$			8	5	30	2	2	
ID$(3, 5, 9)$			9	6	18	2	3	
ID$(3, 5, 10)$			10	7	6	2	4	
ID$(3, 5, 11)$			11	7	12	2	3	
ID$(3, 5, 12)$			12	8	6	3	4	
ID$(4, 4, 1)$	4	4	1	6	24	3	3	
ID$(4, 5, 1)$	4	5	1	7	72	1	4	
ID$(4, 5, 2)$			2	8	48	2	4	
ID$(4, 5, 3)$			3	9	24	3	4	

Table 3.2: Information about studied graph topologies. In table ID(G); $k = \chi(G)$; $n = |V|$ number of vertices; $\mathtt{t}$ enumerates topologies; $|E|$ is the number of edges; degeneracy or in other words number of coloring possibilities; $\min\deg(i)$ minimum and $\max\deg(i)$ maximum degree of the G.
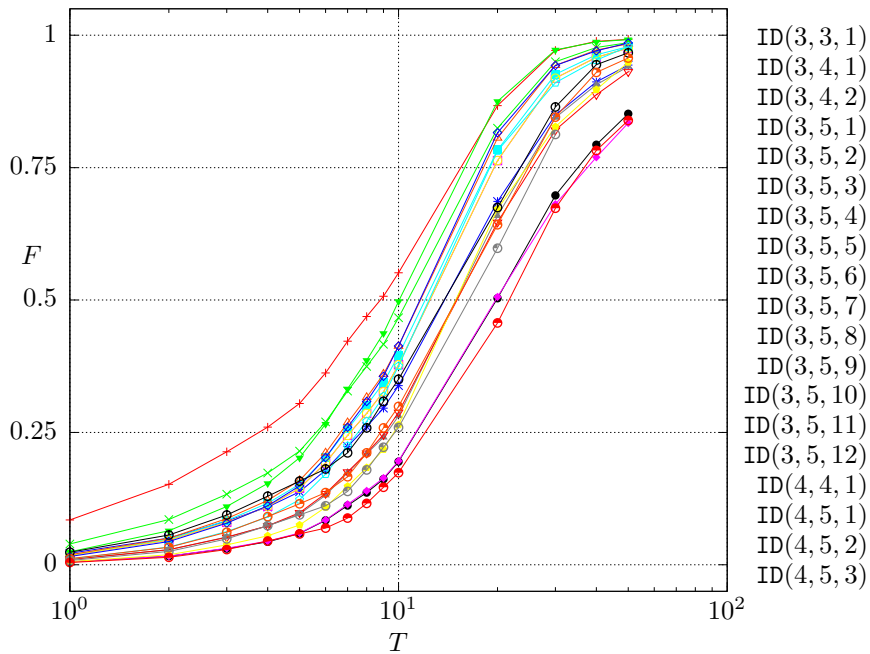
Figure 3.10: Projection F [Eq. (3.7)] as a function of annealing time T for all studied topology cases (without disorder: $W_h = W_J = 0$, $\Delta_i = 2$).
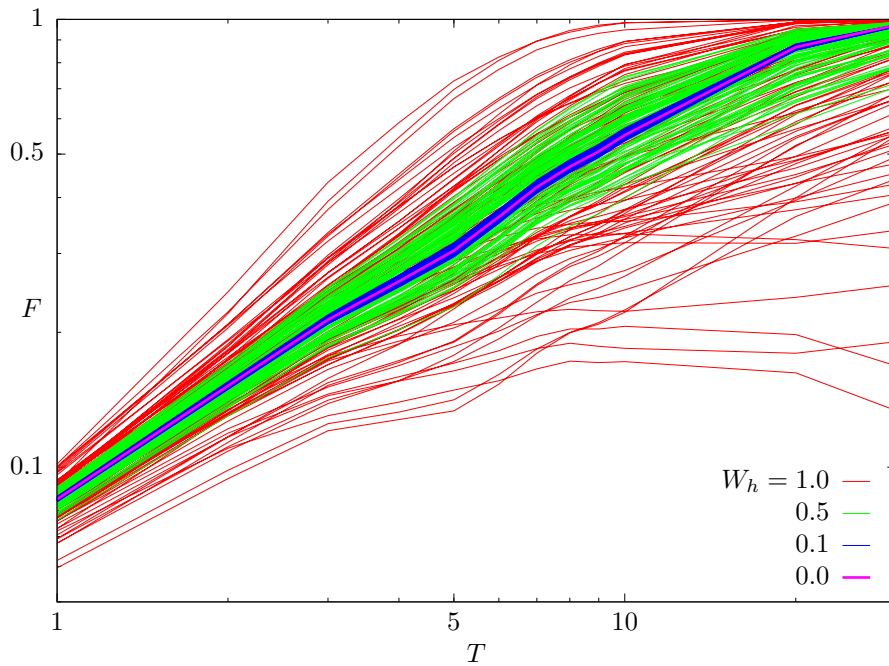

Figure 3.11: 100 realization of projection F [Eq. (3.7)] for the system with disorder h_i as a function of T for case $\text{ID}(3, 3, 1)$. Values of the disorder amplitudes W_h are visible in the plot key. Note: double logarithmic scale. ($\Delta_i = 2$, $W_J = 0$)
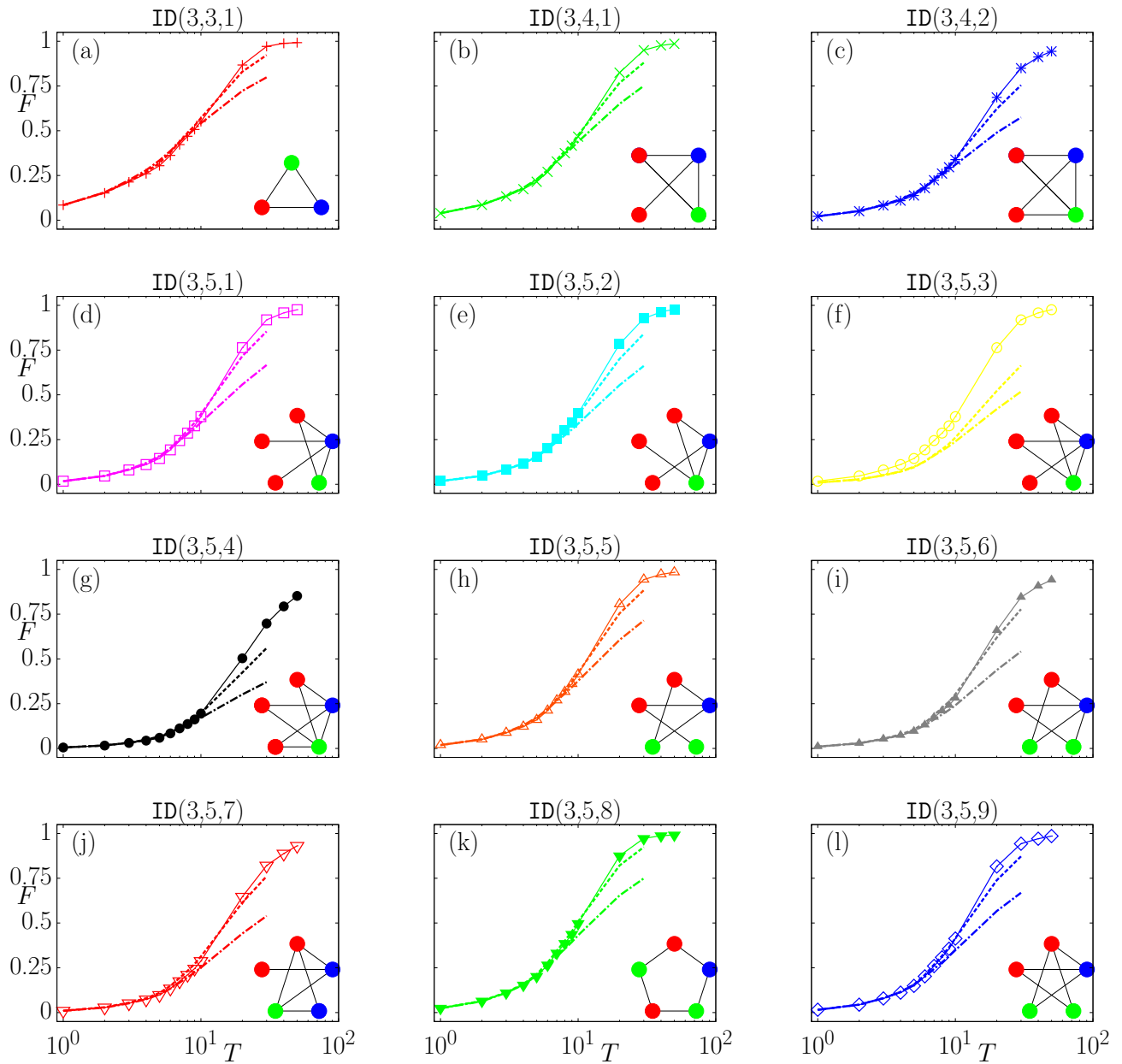
Figure 3.12: Projection F [Eq. (3.7)] as a function of T for all studied cases. Solid line with points corresponds to the results from Fig. 3.10. Dashed line ▬▬▬ corresponds to averaged results for the system with $W_h = 0.5$ and dashed dotted line ▬▬ corresponds to $W_h = 1$. Part 1. ($\Delta_i = 2$, $W_J = 0$)
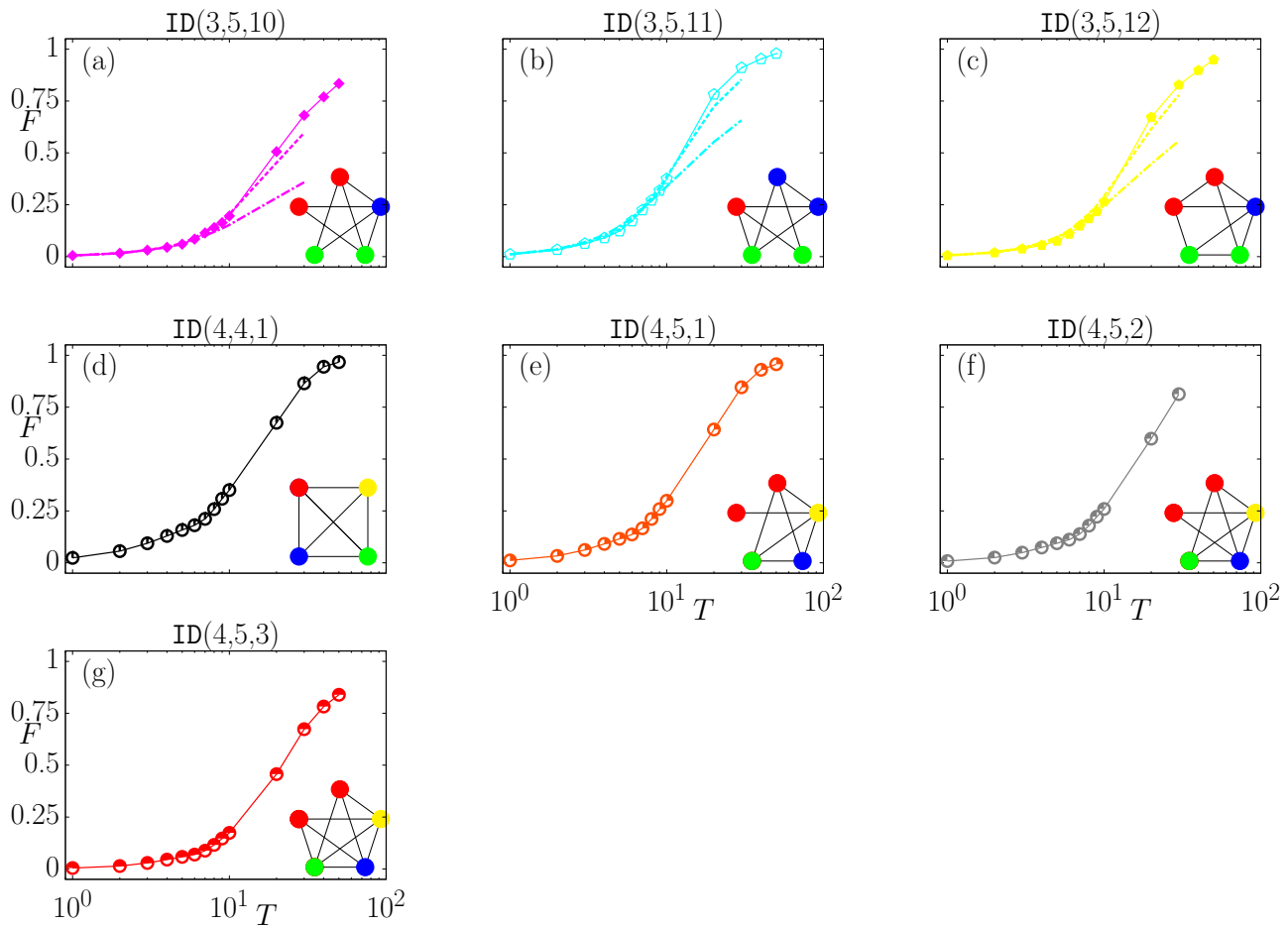
35

Figure 3.13: Projection F [Eq. (3.7)] as a function of T for all studied cases. (a)-(g) solid line with points corresponds to the results from Fig. 3.10. (a)-(c) dashed line ┅ corresponds to averaged results for the system with $W_h = 0.5$ and dashed dotted line ▬·▬ corresponds to $W_h = 1$. Part 2. ($\Delta_i = 2$, $W_J = 0$)
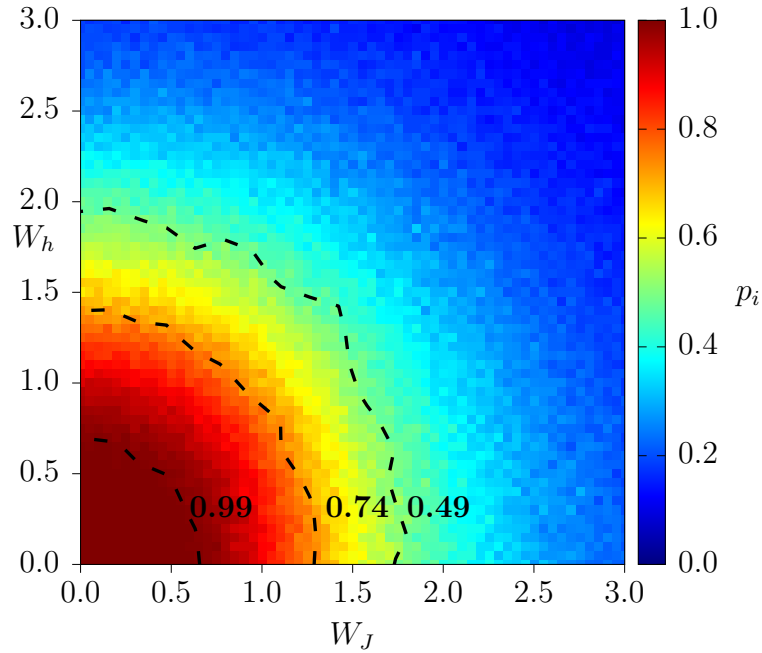
Figure 3.14: Influence of the disorder on ground state properties [Hamiltonian (3.5)]. The plot shows probability p_i that ground state of the disordered system equals to any ground of disorder-free case. Contours show probabilities 0.99, 0.74 and 0.49 respectively. Topology: ID(3,3,1).

3.3.2 Detailed study of selected topologies

In further studies, only selected topologies will be considered. ID(3,3,1) was chosen, because it has the smallest Hilbert space. Additionally, finite-size effects can be systematically studied, due to its similarity to topology of ID(3,5,8) (*odd cycle graph*).

In addition to annealing, properties of a ground states will be investigated. We check how disorder modifies the ground state, i.e., whether the ground state of disordered Ising model is the same as for model without any disorder. The system with disorder was generated, the ground state was found [by solving TISE for disordered Hamiltonian (3.5)] and checked if it is the same as any ground state of the system without any disorder. If it this particular state was found, then it was counted as a success. In Figure 3.14 there is a false-color map showing how W_h and W_J values influence the probability
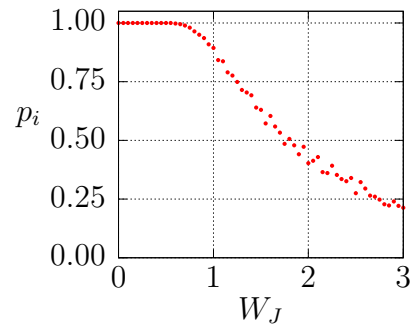

Figure 3.15: Profile at $W_h = 0$ from Figure 3.14.

of success. Each point in the grid corresponds to 1000 realizations. Successful fraction from all realizations are marked with colors. Contours with equal probabilities form a circle-like structure in the plane (W_h, W_J). In Figure 3.15 one can see a selected profile from Figure 3.14. The conclusion may be drawn that disorder in the system, either W_h or W_J, cannot be larger then 1, because then probability, that the ground state will not give correct answer to the original QUBO problem (even in adiabatic limit when $T \to \infty$), will be bigger than 1%.
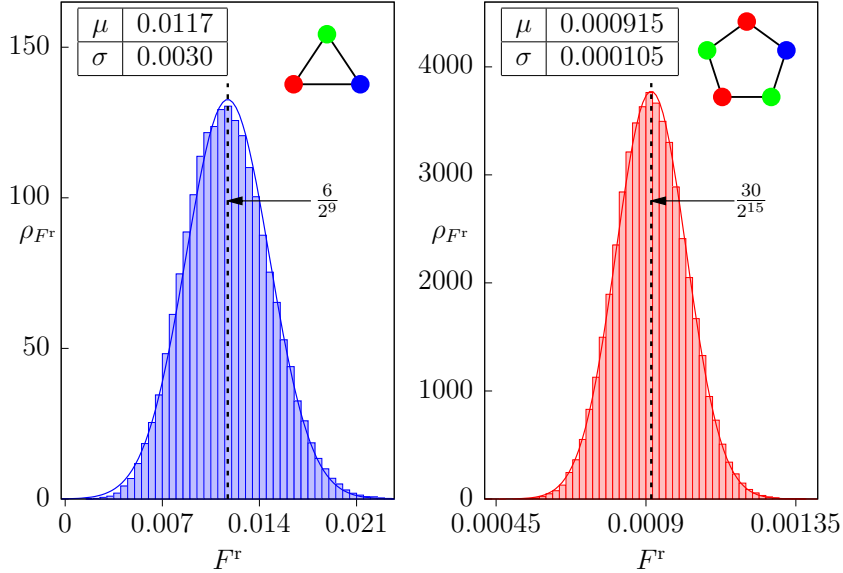

Figure 3.16: Probability density $\rho_{F^r}(F^r)$ of random quantum state projection F^r. Studied topologies are presented in plot.

One can also study projection $F^r = \sum_{i \in \mathbf{gs}} |\langle \psi^r | i \rangle|^2$ of a random state $|\psi^r\rangle$ on the ground state $|i\rangle$ of the disorder-free Ising model, as obtained from the original QUBO. In Figure 3.16 the result of such studies is presented. First complex random state from full Hilbert space was generated respectively for topologies ID(3,3,1) and ID(3,5,8). Next projections of these states on solutions of the graph coloring problems were calculated. This probability of the correct solution should be related to the degeneracy of the ground state of the Ising model and dimensions of the Hilbert space. In fact it is. The ratio of the ground state and Hilbert space dimension is marked by black dashed line with corresponding value pointed out with an arrow. Gaussian distributions $\rho_{F^r}(F^r) = \frac{1}{\sqrt{2\pi\sigma^2}} \exp(-(F^r - \mu)^2/(2\sigma^2))$ managed to fit perfectly the obtained results. In attached tables in the figure mean value μ and standard deviation σ of collected data is displayed. One should be also aware that for bigger system μ and σ are getting approach 0. The random procedure was repeated 10^5 times. Comparing Figs. 3.14 and 3.16 one finds that large overlaps of the ground states for disordered and disorder-free Hamiltonians (see Fig. 3.14) do not arise as accidental events.
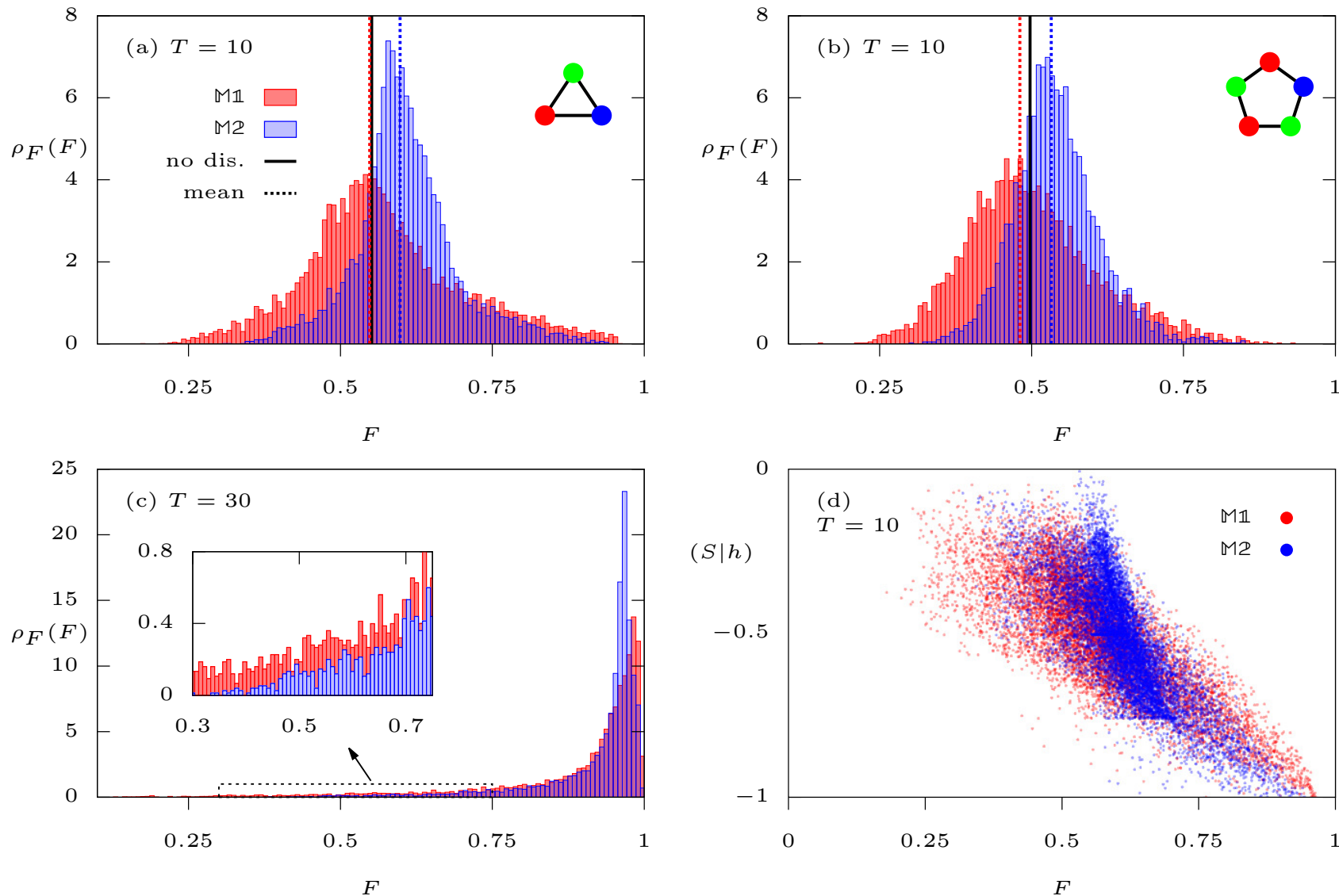
Figure 3.17: (a)-(c) probability density $\rho_F(F)$ for projection F [Eq. (3.7)] for method $\mathbb{M1}$ [Eq. (3.8)] and $\mathbb{M2}$ [Eq. (3.9)]. With vertical lines are marked: (solid) projection value for system without disorder and (dotted) corresponding mean values for disorder cases. In (d) classical inner product $(S|h)$ [Eq. (3.10)] as a function of projection F is presented. Plots (a), (c) and (d) are regarding to same topology presented in (a). Data in (b) are related to topology presented in plot. ($\Delta_i = 2$, $W_J = 0$)

For now on various implementations of disorder will be considered. Since in actual machines one cannot choose arbitrarily parameters for the 'Hamiltonian', some limitations on parameters values should be imposed. Disorder in field h_i not in J_{ij} will be set only. Note that topologies $\text{ID}(3,3,1)$ and $\text{ID}(3,5,8)$ are almost the same. The system without disorder should always have $\tilde{h}_i = k + \frac{1}{2}\deg(i) - 2 = 2$, because all vertices are degree of 2 and $k = 3$. Two different methods were examined:

- method M1:

$$\tilde{h}_i = \begin{cases} 2 + \Delta\tilde{h}_i, & \text{for } \Delta\tilde{h}_i < 0.25; \\ 2.25, & \text{for } \Delta\tilde{h}_i \geqslant 0.25; \end{cases} \qquad (3.8)$$

- method M2:

$$\tilde{h}_i = \begin{cases} 2 + \Delta\tilde{h}_i, & \text{for } \Delta\tilde{h}_i < 0; \\ 2, & \text{for } \Delta\tilde{h}_i \geqslant 0, \ \Delta\tilde{h}_i \in [-\tilde{W}_h, \tilde{W}_h]. \end{cases} \qquad (3.9)$$

$\Delta\tilde{h}_i$ is random variable with flat distribution with amplitude $\tilde{W}_h = 1$. In Figure 3.17 the comparison of these two disorder methods M1 and M2 to system without disorder is presented. In Figure 3.17a-c a probability density $\rho_F(F)$ of projections F [see Eq. (3.7)] for both methods is shown. Figures 3.17a and 3.17b are for $T = 10$. Mean values for both methods are marked with dotted lines. As one can see, method M2 is better, i.e. more results are on the right hand side of non-disorder case, then in M1. The distribution M2 also has smaller variance and its mean value is greater then projection value for system without any disorder (solid line). Method M2 can be used for potentially improving the performance of the QA. In Figure 3.17c results for longer times $T = 30$ are plotted. The highest peak for method M2 is to the left from peak of method M1 for this case, but peak value of method M2 is higher then M1. It is related to distributions 'tails', which can be seen in the inset. However this results for longer times is not very interesting since, relatively short times of annealing with high projection are required. It is interesting to note, that introducing disorder may improve the performance of QA, in that it increases probability of finding the ground state of the original QUBO, which contains no disorder. In order to explain this result we have calculated correlations between $\tilde{h}_i$ and spin configuration S of the ground state of the Ising model. Classical inner product between vector of spin configuration of the ground state $S = [S_i]$ and vector of field $\tilde{h} = [\tilde{h}_i]$ has been used (where $i = 1, \dots, L$):

$$(S|h) = \min_{n \in \mathbf{gs}} \frac{\text{cov}(S^{(n)}, \tilde{h})}{\sigma_{S^{(n)}}\sigma_{\tilde{h}}} = \min_{n \in \mathbf{gs}} \frac{\sum\limits_i (S_i^{(n)} - \langle S \rangle)(\tilde{h}_i - \langle \tilde{h} \rangle)}{\sqrt{\sum\limits_j (S_j^{(n)} - \langle S \rangle)^2}\sqrt{\sum\limits_j (\tilde{h}_j - \langle \tilde{h} \rangle)^2}}, \qquad (3.10)$$

where n enumerates all ground states of the Ising model as derived from QUBO. $\langle x \rangle$ stands for the expectation value: $\langle x \rangle = \frac{1}{N} \sum_{i=1}^{N} x_i$. Minimum of these correlation was taken, because large and positive h_i promotes negative S_i^z so the covariance (3.10) is negative. As one can see in Figure 3.17d, obtained data are strongly correlated. Data with the highest value of projection are the most anti-correlated. One may make a conclusion that disorder in field $\tilde{h}$ can affect the projection F, if values of $\tilde{h}_i$ are set in such way that they promote spin configuration, which represents the solution of QUBO.
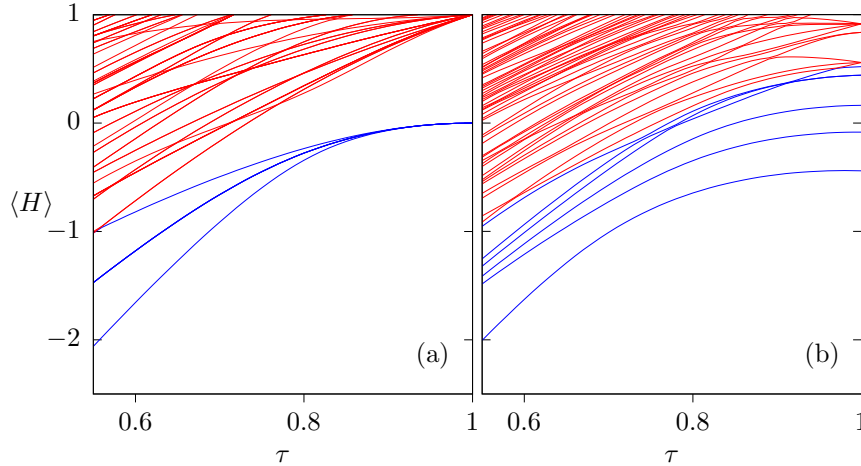

Figure 3.18: Energy spectrum fragment in selection time range τ of evolution process for (a) system without disorder, (b) system with disorder $\mathbb{M}2$ [Eq. (3.9)]. (Topology: $\mathtt{ID}(3,3,1)$, $\Delta_i = 2$)

Again one can try to use LZF for describing studied phenomenon. In Figure 3.18 we show the energy spectrum during the evolution [Eq. (3.6)] for two different cases. In Figure 3.18a there is the result for the system without disorder and in Figure 3.18b selected realization with disorder $\mathbb{M}2$ [Eq. (3.9)]. In the first case (Fig. 3.18a) ground state is 6 times degenerated at time $\tau = 1$. Due to the minimum value of the gap $\beta = 0$, application LZF for this case may not work properly. However, for the second case (Fig. 3.18b) there is no degeneracy of the ground state at $\tau = 1$. In case from Fig. 3.18b, LZF should work reasonably if the gap is properly large. One may propose some other energy gap for approximation by LZF (e.g. difference between ground state energy and the first non-degenerated state energy at $\tau = 1$ for disorder-free case). However, energy levels spectrum during the evolution is very complicated and it is very hard to find other quantity which can be calculated then gap between two the lowest energy states. In Figure 3.19 the relation between fitted parameters β, α, τ_0 for LZF (same Hamiltonian as was used in Section 2.3.3), calculated negated transition probability $\widetilde{\mathcal{P}}_{LZ}^{T}$ [Eq. (2.7)] and projection F [Eq. (3.7)] for 10^4 disorder ($\mathbb{M}2$) realizations is demonstrated. As one can see in Figure 3.19d, for some systems settings, for which obtained projection is
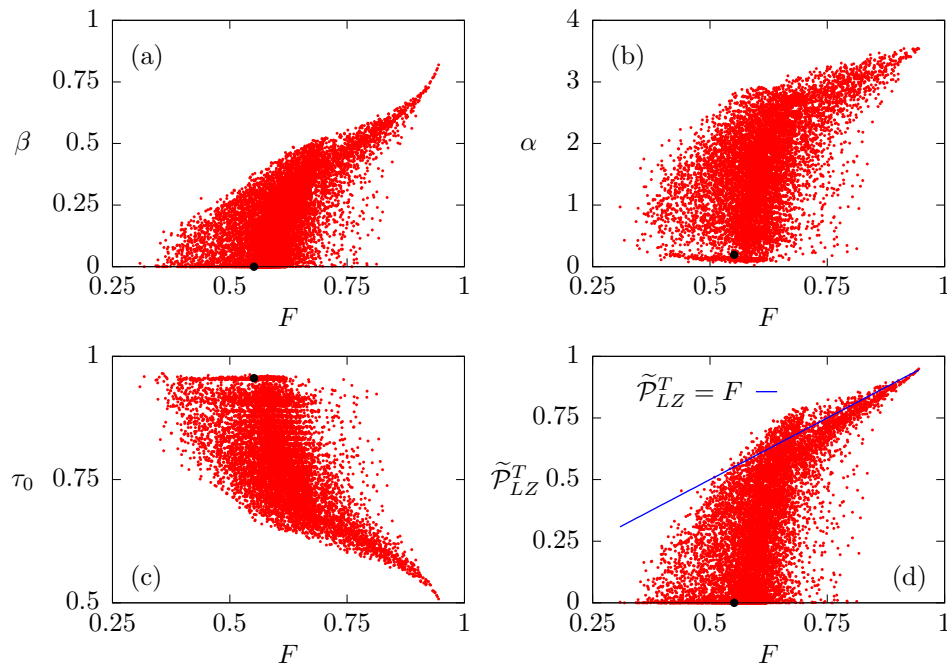
Figure 3.19: Fitted parameters for LZF [same Hamiltonian (2.4) as was used in Section 2.3.3, $\widetilde{\mathcal{P}}_{LZ}^T$ [Eq. (2.7)], F [Eq. (3.7)] for 10^4 realizations of disorder $\mathbb{M}2$ [Eq. (3.9), topology: $\mathbb{ID}(3,3,1)$]. Black dot corresponds to disorder-free case. ($\Delta_i = 2$, $\tilde{W}_h = 1$, $W_J = 0$, $T = 10$)

large (about $F \geqslant 0.75$), the evolution process can be well approximated with LZF. Result for disorder-free case is marked with black dot.

Conclusions

In summary, the thesis provides the reader theoretical background and (hopefully future) applications for adiabatic quantum computers. The results are promising with future research opportunities.

The main purpose of the thesis is to discuss adiabatic quantum computations using Hamiltonians which are relevant for the D-Wave quantum annealers. We have considered the most general form of the spin Hamiltonian, which cannot be mapped on a system of noninteracting particles. The latter assumption poses a challenge since one needs to study the non-equilibrium dynamics of generic interacting quantum systems. However, in order to test and benchmark our approach, we have shown that our results accurately reproduce the data for the simplified case when one may avoid the complexity of many–body interactions. The original studies within the thesis are focused on disordered systems. In this way, we have simulated the situation which is most probably relevant for the D-Wave annealers. Namely, the D-Wave annealers may still be imperfectly tuned on the hardware level. As a consequence, parameters of the Hamiltonian which defines the quantum dynamics may differ from the values which are set within the program being run on the D-Wave annealer. For a selected realizations of the quenched disorder, the adiabatic dynamics turns out to be more robust than for original disorder-free model. Therefore, particularly tuned weak disorder may even improve the performance of the D-Wave annealers. It is the main novel result reported in the present thesis.

In the future, one needs to carry out more general consideration and compare the theoretical predictions with results obtained directly from real adiabatic quantum computer. Further work is necessary for our better knowledge on quantum nature and for the improvement of our technology.

Appendix A

Numerical methods

In this appendix numerical methods will be described which were used to obtain results in this thesis. The most three important methods are briefly described:

- Lanczos method for finding eigenvalues/eigenvectors for large sparse matrices;

- Chebyshev propagation a numerical method for solving differential equations, especially Schrödinger equation;

- Adjacency matrix – data structure storage format for graph topology.

A.1 Lanczos method

Lanczos method [44–47] is a method, based on the *power method* [47, 48], for finding the lowest eigenvalues. Main idea behind this method is to transform symmetric (or hermitian) matrix $[H_{ij}]$ (rank $H = n$) into tridiagonal form $[T_{ij}]$ (rank $T = k$). Algorithm starts from random vector $|f_0\rangle$ and next, by iterative steps, subsequent states $\{|f_i\rangle\}_{i=0}^{k-1}$ are generated:

$$|f_{m+1}\rangle = H|f_m\rangle - a_m|f_m\rangle - b_{m-1}|f_{m-1}\rangle,$$

where here[1] a_m, b_{m-1} can be calculated by the following relations:

$$a_m = \frac{\langle f_m|H|f_m\rangle}{\langle f_m|f_m\rangle};$$

$$b_{m-1} = \frac{\langle f_m|f_m\rangle}{\langle f_{m-1}|f_{m-1}\rangle}.$$

---

[1]Naturally $b_{-1} = 0$.

44

This construction guarantees that set of $\{|f_i\rangle\}$ is orthogonal. Using this result, one can transforms H into T using normalized vector $|f_m\rangle$:

$$|\phi_m\rangle = \frac{|f_m\rangle}{\sqrt{\langle f_m|f_m\rangle}};$$

$$[T_{mm}] = \langle \phi_m|H|\phi_m\rangle = a_m;$$

$$[T_{m-1,m}] = \langle \phi_{m-1}|H|\phi_m\rangle = \sqrt{b_{m-1}}.$$

The matrix $[T_{ij}]$ takes the following tridiagonal form:

$$[T_{ij}] = \begin{pmatrix} a_0 & \sqrt{b_0} & & & 0 \\ \sqrt{b_0} & a_1 & \sqrt{b_1} & & \\ & \sqrt{b_1} & \ddots & \ddots & \\ & & \ddots & a_{k-1} & \sqrt{b_{k-1}} \\ 0 & & & \sqrt{b_{k-1}} & a_k \end{pmatrix}.$$

After k iterations and filling elements of the matrix $[T_{ij}]$ one can diagonalize it to obtain approximate k eigenvalues of matrix H. The most important advantages of this approach is the fact that eigenvalues from the energy spectrum edges are obtained in only a few steps of iterations ($\sim 10^2$). There is no need[2] to transform all n states, very small fraction ($k \ll n$) of n is enough to obtain convergence of the ground state. Since, the largest and the smallest eigenvalues are most interesting, this algorithm is very useful.

A.2 Chebyshev propagation

Chebyshev propagation is a method for solving differential equations based on Chebyshev polynomials properties. Chebyshev polynomial can be constructed by the following recurrence definition [49]:

$$T_k(x) = 2xT_{k-1}(x) - T_{k-2}(x), \tag{A.1}$$

and with initial conditions: $T_0(x) = 1$, $T_1(x) = x$, where $x \in [-1, 1]$. Since Chebyshev polynomials create set of orthogonal basis [49] one can expand any smooth continuous function $f(x)$ on interval $x \in [-1, 1]$ by the following expression:

$$f(x) = \sum_{k=0}^{\infty} c_k T_k(x) = \alpha_0 + 2\sum_{k=1}^{\infty} \alpha_k T_k(x), \tag{A.2}$$

where here $c_k = \frac{\langle f(x)|T_k(x)\rangle}{\langle T_k(x)|T_k(x)\rangle}$, with inner-product $\langle f|g\rangle$ defined as:

---

[2]To many iteration may cause the *ghost state* effect – errors.

$$\langle f|g\rangle = \frac{1}{\pi}\int\limits_{-1}^{1}\mathrm{d}x\ \frac{1}{\sqrt{1-x^2}}f(x)g(x).$$

General solution to Schrödinger Equation (1.4) can be written as follows:

$$|\psi(t)\rangle = U(0,t)|\psi(0)\rangle,$$

where here $U(0,t)$ is time propagator operator. One can calculate U operator by the formula:

$$U(0,t) = \hat{T}_\tau \exp\left(-i\int\limits_{0}^{t}\mathrm{d}\tau\ \hat{H}(\tau)/\hbar\right),$$

where $\hat{T}_\tau$ is chronological operator. Operator $U(0,t)$ can be expanded in a product sequence:

$$U(0,t) = \lim_{\delta t\to 0}U(t-\delta t)\cdots U(\delta t,2\delta t)U(0,\delta t).$$

Assuming that Hamiltonian $\hat{H}$ is constant within very small time window $[t_n, t_n + \delta t]$, solution to Schrödinger equation can be found by iterative steps on finite set of times: $\{t_n : t_n = n\delta t\}_{n=0}^{N}$:

$$|\psi(t_n)\rangle = e^{-i\hat{H}(t_n)\delta t/\hbar}|\psi(t_{n-1})\rangle. \qquad (A.3)$$

The next step is to expand operator $e^{-i\hat{H}(t_n)\delta t/\hbar}$ in a Chebyshev polynomial basis. One can easily find that coefficients α_k of function $f(x) = e^{-ixt}$ in Chebyshev polynomial basis are given by:

$$\alpha_k(t) = (-i)^k J_k(t), \qquad (A.4)$$

where $J_k(t)$ are Bessels function of the first kind. Using iterative property (A.1), series expansion (A.2) and formula for evolution (A.3) one can easily evolve system of given Hamiltonian $\hat{H}$ with following iterative method [50, 51]:

$$|\nu_0\rangle = |\psi(t_{n-1})\rangle;$$
$$|\nu_1\rangle = \tilde{H}|\psi(t_{n-1})\rangle;$$
$$|\nu_k\rangle = 2\tilde{H}|\nu_{k-1}\rangle - |\nu_{k-2}\rangle;$$

$$|\psi(t_n)\rangle = e^{-ib\delta t/\hbar}\left(\alpha_0(a\delta t/\hbar)|\nu_0\rangle + 2\sum_{k=1}^{\infty}\alpha_k(a\delta t/\hbar)|\nu_k\rangle\right);$$

where $\tilde{H} = \frac{1}{a}(\hat{H} - b\mathbb{1})$ and a,b are scaling parameters. Since Chebyshev polynomials are well defined on range $x \in [-1,1]$, then we should rescale our Hamiltonian spectrum to fit that boundaries.

A.3   Adjacency matrix

It is very useful to represent graph G in adjacency matrix A_{ij} representation [36]. This matrix contains 0 or 1 values. If vertices i and j are connected then $A_{ij} = 1$ otherwise $A_{ij} = 0$. Below example from Figure 3.2 is considered with written down corresponding adjacency matrix $[A_{ij}]$ and vector of all degree of vertices $[\deg(i)]$:
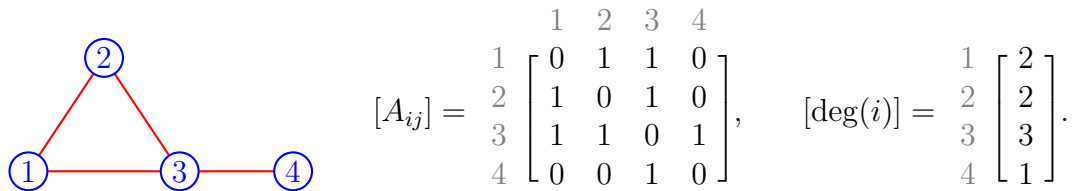
$$
[A_{ij}] = \begin{matrix} & \begin{matrix} 1 & 2 & 3 & 4 \end{matrix} \\ \begin{matrix} 1 \\ 2 \\ 3 \\ 4 \end{matrix} & \begin{bmatrix} 0 & 1 & 1 & 0 \\ 1 & 0 & 1 & 0 \\ 1 & 1 & 0 & 1 \\ 0 & 0 & 1 & 0 \end{bmatrix} \end{matrix}, \qquad [\deg(i)] = \begin{matrix} 1 \\ 2 \\ 3 \\ 4 \end{matrix} \begin{bmatrix} 2 \\ 2 \\ 3 \\ 1 \end{bmatrix}.
$$

Figure A.1: Example graph with corresponding adjacency matrix representation and vector containing degree of each vertex.

This matrix representation is very useful if one want to calculate, e.g., the degree $\deg(i)$ of each vertex. To achieve this, one should simply sum all entries in a specific row/column which correspond to selected vertex i. On the other hand if information about vector of degree of all vertices is available then one can easily calculate the total number of edges using famous handshaking lemma:

> **Lemma 1: Handshaking lemma**
>
> For any finite undirected graph G with vertex set V and edges E:
> $$\sum_{i \in V} \deg(i) = 2|E|.$$

Proof of this lemma is quite obvious: when degrees of all vertices are added, one counts every edge twice, so one should divide the sum by 2 to obtain total number of edges $|E|$ in graph G.

Interesting interpretation has n-th power of adjacency matrix A^n [35]. Value of element $[(A^n)_{ij}]$ is a number of paths of length n from i to j. Such construction allows to (for simple structures like *trees*) determine next nearest neighbors $\langle\langle i, j \rangle\rangle$ for nearest neighbors $\langle i, j \rangle$ after some operations.

47

Appendix B

Landau-Zener transition

This appendix contains simple derivation and some comments of Landau-Zener transition. All calculations and informations are based on papers: [52–55].

B.1 Landau-Zener derivation

Landau-Zener transition is a simple model of transition of 2-level system $\{|\uparrow\rangle, |\downarrow\rangle\}$. The system can be described with the following time-dependent Hamiltonian:

$$\hat{H}(t) = \frac{1}{2}\left(\alpha t \sigma^z + \beta \sigma^x\right) = \frac{1}{2}\begin{pmatrix} \alpha t & \beta \\ \beta & -\alpha t \end{pmatrix}. \tag{B.1}$$

One can easily find eigenvalues of such Hamiltonian:

$$\hat{H}\psi = E\psi;$$

$$(\hat{H} - E\mathbb{1})\psi = 0;$$

$$\det(\hat{H} - E\mathbb{1}) = 0;$$

$$\det\left[\frac{1}{2}\begin{pmatrix} \alpha t - E & \beta \\ \beta & -\alpha t - E \end{pmatrix}\right] = 0;$$

$$\frac{1}{4}\left(-(\alpha t - E)(\alpha t + E) - \beta^2\right) = 0;$$

$$\frac{1}{4}\left(\alpha^2 t^2 + \beta^2\right) = E^2.$$

Finally our system has eigenenergies:

$$E = \pm\frac{1}{2}\sqrt{(\alpha t)^2 + \beta^2}. \tag{B.2}$$
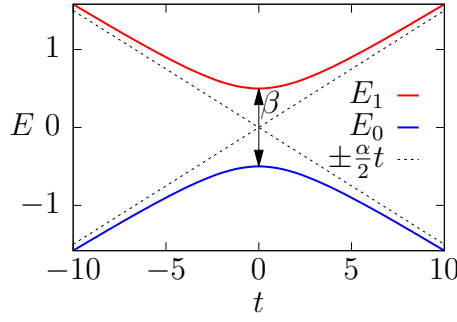
Figure B.1: Example Landau-Zener Hamiltonian energy spectrum in time t function (parameters: $\alpha = 0.3; \beta = 1$).

Let's write state $|\psi(t)\rangle$ in same basis like in Hamiltonian (B.1):

$$|\psi(t)\rangle = c_1(t)|\uparrow\rangle + c_2(t)|\downarrow\rangle. \tag{B.3}$$

Now by putting this state to Schrödinger equation:

$$i|\dot{\psi}(t)\rangle = \hat{H}|\psi(t)\rangle;$$

$$i\begin{pmatrix} \dot{c}_1(t) \\ \dot{c}_2(t) \end{pmatrix} = \frac{1}{2}\begin{pmatrix} \alpha t & \beta \\ \beta & -\alpha t \end{pmatrix}\begin{pmatrix} c_1(t) \\ c_2(t) \end{pmatrix} = \frac{1}{2}\begin{pmatrix} \alpha t c_1 + c_2 \beta \\ \beta c_1 - \alpha t c_2 \end{pmatrix}. \tag{B.4}$$

From Equation (B.4) one can get the following set of equations:

$$\begin{cases} \dot{c}_1 = -\frac{i}{2}\left(\alpha t c_1 + \beta c_2\right); \\ \dot{c}_2 = -\frac{i}{2}\left(\beta c_1 - \alpha t c_2\right). \end{cases} \tag{B.5}$$

Next, the second derivative of equation for $\dot{c}_1$ from Eq. (B.5) is calculated:

$$\ddot{c}_1 = -\frac{i}{2}\left(\alpha c_1 + \alpha t \dot{c}_1 + \beta \dot{c}_2\right).$$

After that, using the second equation from set of equations (B.5):

$$\ddot{c}_1 = -\frac{i}{2}\alpha c_1 - \frac{i}{2}\alpha t \dot{c}_1 - \frac{\beta}{4}\left(\beta c_1 - \alpha t c_2\right).$$

Term c_2 from the equation can be replaced from the first equation from set of equations (B.5):

$$\ddot{c}_1 = -\frac{i}{2}\alpha c_1 - \frac{i}{2}\alpha t \dot{c}_1 - \frac{\beta^2}{4}c_1 + \frac{\alpha t}{2}\left(i\dot{c}_1 - \frac{1}{2}\alpha t c_1\right) =$$

$$= -\frac{i}{2}\alpha c_1 - \frac{i}{2}\alpha t \dot{c}_1 - \frac{\beta^2}{4}c_1 + \frac{i}{2}\alpha t \dot{c}_1 - \frac{\alpha^2 t^2}{4}c_1.$$

49

One can end with second order differential equation for only $\ddot{c}_1, c_1$:

$$\ddot{c}_1 + \left(\frac{i\alpha}{2} + \frac{\beta^2}{4} + \left(\frac{\alpha t}{2} \right)^2 \right) c_1 = 0. \tag{B.6}$$

Using substitution $c_1 = |c_1| \exp[-i\varphi(t)]$ in Equation (B.6), where $\varphi(t)$ is some real function:

$$|c_1|e^{-i\varphi(t)}(-i\dot{\varphi}(t))^2 + |c_1|e^{-i\varphi(t)}(-i\ddot{\varphi}(t)) + \left(\frac{i\alpha}{2} + \frac{\beta^2}{4} + \left(\frac{\alpha t}{2} \right)^2 \right) |c_1|e^{-i\varphi(t)} = 0;$$

$$-\dot{\varphi}(t)^2 - i\ddot{\varphi}(t) + \frac{i\alpha}{2} + \frac{\beta^2}{4} + \left(\frac{\alpha t}{2} \right)^2 = 0.$$

Now, separation into real and imaginary part (because all parameters are real) is done:

$$\begin{cases} \ddot{\varphi}(t) = \frac{\alpha}{2}; \\ \dot{\varphi}(t) = \pm \frac{1}{2}\sqrt{(\alpha t)^2 + \beta^2}. \end{cases} \tag{B.7}$$

The second equation from set of equations (B.7) one can transform into the following form:

$$\dot{\varphi} = \pm \frac{1}{2}\sqrt{(\alpha t)^2 + \beta^2} = \pm \frac{1}{2}\alpha|t|\sqrt{1 + \frac{\beta^2}{\alpha^2 t^2}}.$$

This expression can be further simplified with condition $t \to \pm\infty$:

$$(\dot{\varphi})_{t\to\pm\infty} = \frac{1}{2}\alpha t \sqrt{1 + \frac{\beta^2}{\alpha^2 t^2}}. \tag{B.8}$$

Since Taylor expansion of $\sqrt{1+x} \approx 1 + \frac{1}{2}x$, then it can be approximated with the following:

$$(\dot{\varphi})_{t\to\pm\infty} \approx \frac{1}{2}\alpha t + \frac{1}{4}\frac{\beta^2}{\alpha t}. \tag{B.9}$$

With this result one can calculate the following:

$$\left(\frac{\dot{c}_1}{c_1} \right)_{t\to\pm\infty} = \left(\frac{|c_1|e^{-i\varphi}(-i\dot{\varphi})}{|c_1|e^{-i\varphi}} \right)_{t\to\pm\infty} = -i\dot{\varphi}_{t\to\pm\infty}. \tag{B.10}$$

Since $\frac{\dot{c}_1}{c_1}$ is well-behaved on real domain then it can be expanded to complex plane and by using Cauchy integral theorem[56]:

$$\int\limits_{-\infty}^{+\infty} dt \frac{\dot{c}_1(t)}{c_1(t)} = -\int\limits_{C} dz \frac{\dot{c}_1(z)}{c_1(z)}, \tag{B.11}$$

where C is integral contour, which is visualized on Figure B.2. The left hand side of equation (B.11) can be easily obtained:

$$\int\limits_{-\infty}^{+\infty} dt \frac{\dot{c}_1}{c_1} = \int\limits_{-\infty}^{+\infty} dt \frac{dc_1}{dt}\frac{1}{c_1} = \int\limits_{-\infty}^{+\infty} \frac{dc_1}{c_1} = \ln \frac{c_1(+\infty)}{c_1(-\infty)}. \tag{B.12}$$
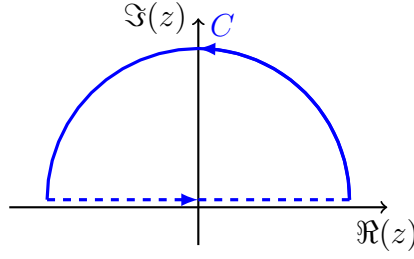
Figure B.2: Integration contour C.

This contour C can be parametrized with $z = Re^{i\theta}$, where $R \to \infty$ and $\theta \in [0, \pi]$. Using Equations (B.9),(B.10) one can calculate the right hand side of equation (B.11):

$$-\int_C \mathrm{d}z \frac{\dot{c}_1(z)}{c_1(z)} = -\int_C \mathrm{d}z \left(\frac{\dot{c}_1(z)}{c_1(z)}\right)_{|z|\to\infty} = i\int_C \mathrm{d}z \left(\tfrac{1}{2}\alpha z + \tfrac{1}{4}\tfrac{\beta^2}{\alpha z}\right) =$$

$$= i \lim_{R\to\infty} \int_0^\pi \mathrm{d}\theta \left(\tfrac{i}{2}R^2 e^{2i\theta} + \tfrac{i}{4}\tfrac{\beta^2}{\alpha}\right) = -\tfrac{\pi\beta^2}{4\alpha}\bigg|_0^\pi = -\tfrac{\pi\beta^2}{4\alpha}. \qquad \text{(B.13)}$$

Now simply by connecting the left hand side [Equation (B.12)] with the right hand side [Equation (B.13)]:

$$\ln \frac{c_1(+\infty)}{c_1(-\infty)} = -\tfrac{\pi\beta^2}{4\alpha};$$

$$c_1(+\infty) = c_1(-\infty) \exp(-\tfrac{\pi\beta^2}{4\alpha}). \qquad \text{(B.14)}$$

The probability of Landau-Zener transition $\mathcal{P}_{LZ}$ is given by the formula:

$$\mathcal{P}_{LZ} = |c_1(+\infty)|^2 = \underbrace{|c_1(-\infty)|^2}_{1} \exp(-\tfrac{\pi\beta^2}{2\alpha}) = \exp(-\tfrac{\pi\beta^2}{2\alpha}). \qquad \text{(B.15)}$$

B.2   Numerical results

To verify this analytical solution [Equation (B.15)], similar Hamiltonian was studied like in Equation (B.1) using numerical methods which was described in Appendix A:

$$\hat{H} = \frac{1}{2}\begin{pmatrix} \frac{\alpha}{T}t & \beta \\ \beta & -\frac{\alpha}{T}t \end{pmatrix}. \qquad \text{(B.16)}$$

Since numerically one cannot obtain evolution from $t = -\infty$ to $t = +\infty$, evolution was proceed in finite time range $t \in [-T, T]$. As initial condition to Schrödinger equation ground state of the matrix at $t = -T$ was put. This little
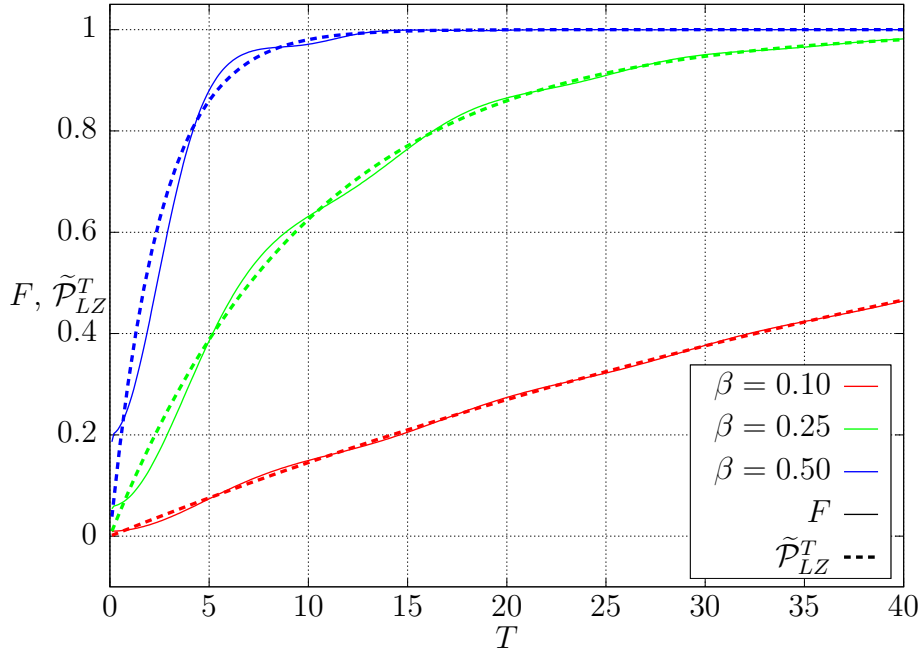
Figure B.3: Comparison numerical results to analytical Landau-Zener formula from Equation (B.15) (parameters: $\alpha = 1$, β, T are visible in plot.)

modification in Hamiltonian (B.16) guarantees that for any T evolution always starts from the same state. In Figure B.3 a comparison between numerical and analytical solution (which is only correct in $T \to \infty$) is presented. In this figure one can see projection $F = |\langle \psi_0 | \psi \rangle|^2$ (solid line) as a function of total evolution time T, where $|\psi_0\rangle$ is a ground state for Hamiltonian (B.16) at $t = T$ and $|\psi\rangle$ is a state, which is obtained from Schrödinger equation (TDSE). Negated probability solution from Equation (B.15) is plotted with dashed lines with proper scaling of α parameter: $\tilde{\mathcal{P}}_{LZ}^T = 1 - \exp(-\frac{\pi \beta^2}{2\alpha} T)$. As one can see Landau-Zener formula giving (almost) same result to numerical exact evolution even for $T < \infty$.

Appendix C

Experiments on DW-2000Q

In this appendix, the preliminary results realized on real physical quantum annealer are presented. However, all information here is in the first phase of the study. The authors are very grateful for D-Wave Systems for providing access to their machines.

Annealing on DW-2000Q

In this section topology ID(3,3,1) will be studied again, although on real adiabatic quantum computer. In general, process of embedding to chimera topology can be very difficult. In Figure C.1 embedding process of graph coloring problem is introduced. Graph, which has 3 vertices (Fig. C.1a), is represented by 9 qubits in Ising model (Fig. C.1b), and it can be realized on chimera topology using 20 qubits (Fig. C.1c). D-Wave System provides a software, which carries out this embedding using heuristic method.

Studying disorder influence on the effectiveness of QA using D-Wave's computer can be problematic. At each programing cycle user defines parameters

(a) $G(E,V)$ (b) Ising mapping   (c) Chimera embedding
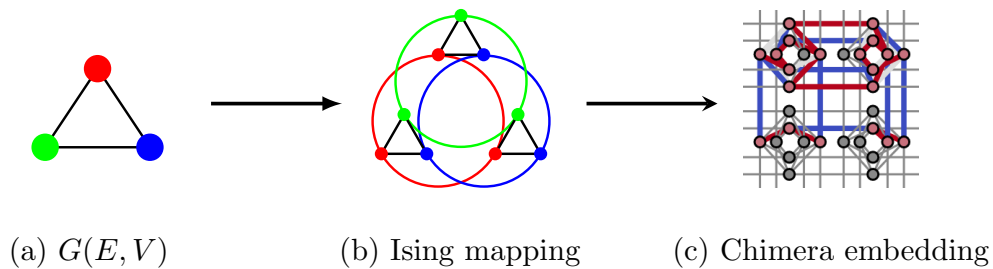
Figure C.1: Representation of: (a) studied 3-colorable graph $G(E,V)$ case ID(3,3,1); (b) same problem mapped into Ising model and (c) an example embedding on chimera topology.
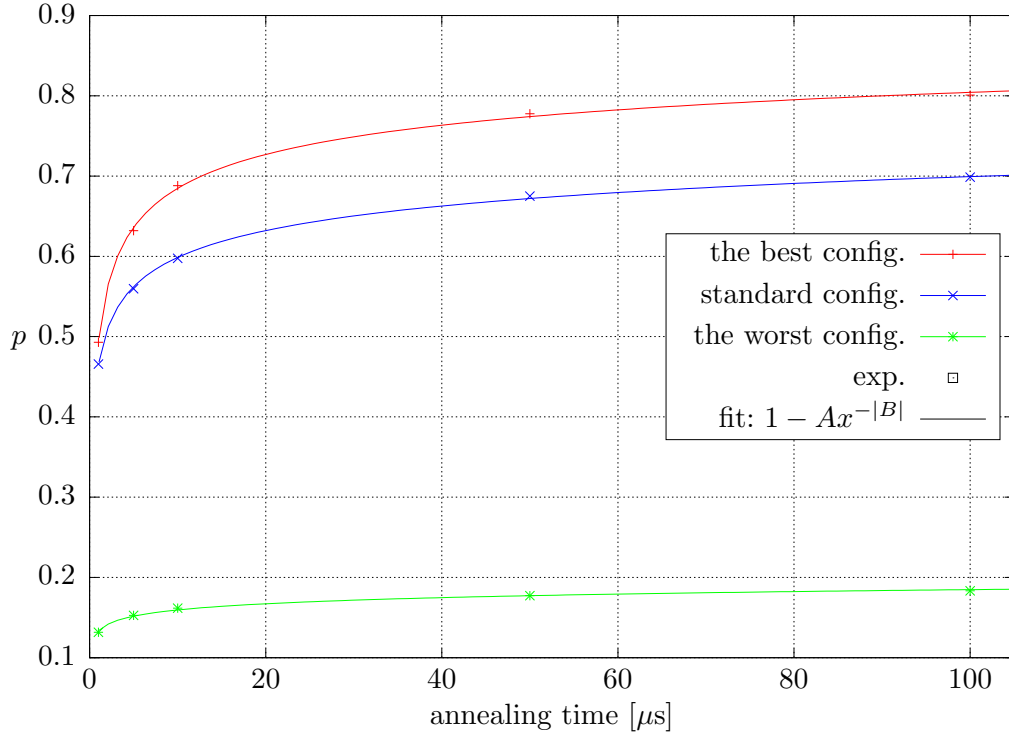
Figure C.2: Averaged fraction of correct answers p obtained on DW-2000Q machine (with points) as a function of annealing time and corresponding fit (with lines). Different cases are marked with colors: blue – standard parameter setting; red/green – the best/worst configuration, which is found with theoretical calculations for disordered systems. [Hamiltonian (3.5), topology `ID(3,3,1)`, energy scale factor 0.2, 10^2 runs with 10^4 realizations]

h_i and J_{ij} and since hardware has limited precision, actual values of these parameters are slightly deviated from input values. Nevertheless we managed to study selected configurations, which were obtained for system with disorder J_{ij} and h_i, on actual D-Wave annealer DW-2000Q. The best and the worst configuration from previous studies for topology `ID(3,3,1)` were chosen for the verification. To do better measurement of annealing time dependence, the hole energy range of the parameters was scaled by factor 0.2. Probability of correct answer p after annealing was measured, i.e. in one run of 10 000 realizations ratio between correct and all results was calculated. 100 of such runs with 10 000 realizations were performed and then the final result was calculated by averaging all samples for proper annealing time. As one can see in Figure C.2, on real quantum machine the results are quite promising. We observed performance improvement for the best case from theoretical calculations and performance failure for the worst case. This investigation, in some way, can be considered as an experimental authentication.

List of Figures

Glossary

Acronyms

AQC   Adiabatic Quantum Computing

BQP   Bounded error quantum polynomial time

CPU   Central processing unit

LZF   Landau-Zener formula

OBC   Open boundary conditions

P   Polynomial time
#P   Number **P**
NP   Nondeterministic   polynomial time
NPC   **NP** complete

QA   Quantum annealing
QPU   Quantum processing unit
QUBO Quadratic unconstrained binary optimization

SA   Simulated annealing

TDSE   Time-dependent   Schrödinger equation [Eq. (1.4)]
TISE   Time-independent   Schrödinger equation [Eq. (1.5)]

List of Symbols

$\mathcal{O}$ big o notation
σ_i^k Pauli operators $(k = x, y, z)$
gs   set of all ground states
$|\psi\rangle$ ket state

$\langle A \rangle$ expectation value

$\hat{H}$ Hamiltonian
$\mathcal{H}$ Hilbert space

$\mathcal{P}_{LZ}$ LZF transition probability

$N_{\mathbf{kinks}}$ number of kinks
χ chromatic number
L number of qubits

$\otimes$ tensor product
$\dot{x}$ time derivative
$\lfloor x \rfloor$ floor function

$\rho_\xi(x)$ probability density
F projection

$\mathbb{R}$ set of real numbers
$\mathbb{C}$ set of complex numbers
$\mathbb{1}$ identity matrix

t time of evolution
T total time of evolution
τ normalized time of evolution

S_i spin-$\frac{1}{2}$ variable
X_i binary variable

Bibliography

[1] Gordon E Moore. Cramming more components onto integrated circuits, Reprinted from Electronics, volume 38, number 8, April 19, 1965, pp. 114 ff. *IEEE Solid-State Circuits Society Newsletter*, 20(3):33–35, 2006. 1

[2] M. Mitchell Waldrop. The chips are down for Moore's law. *Nature*, 530(7589):144–147, 2016. 1

[3] Paul Benioff. The computer as a physical system: A microscopic quantum mechanical Hamiltonian model of computers as represented by Turing machines. *Journal of statistical physics*, 22(5):563–591, 1980. 1

[4] Yu I Manin. Vychislimoe i nevychislimoe (Computable and Noncomputable), Moscow: Sov, 1980. 1

[5] Richard P Feynman. Simulating physics with computers. *International journal of theoretical physics*, 21(6):467–488, 1982. 1

[6] David Deutsch and Richard Jozsa. Rapid solution of problems by quantum computation. In *Proceedings of the Royal Society of London A: Mathematical, Physical and Engineering Sciences*, volume 439, pages 553–558. The Royal Society, 1992. 1

[7] Lov K Grover. A fast quantum mechanical algorithm for database search. In *Proceedings of the twenty-eighth annual ACM symposium on Theory of computing*, pages 212–219. ACM, 1996. 1

[8] Peter W Shor. Polynomial-time algorithms for prime factorization and discrete logarithms on a quantum computer. *SIAM review*, 41(2):303–332, 1999. 1

[9] Michael A Nielsen and Isaac L Chuang. Quantum computation and quantum information. *Quantum*, 546:1231, 2000. 2, 4, 6, 7

[10] Isaac L Chuang, Neil Gershenfeld, and Mark Kubinec. Experimental implementation of fast quantum searching. *Physical review letters*, 80(15):3408, 1998. 3

[11] IBM. *IBM Builds Its Most Powerful Universal Quantum Computing Processors*. Accessed: 2018-01-25. 3

[12] D-Wave Systems Inc. *The D-Wave 2000Q^{TM} Quantum Computer Technology Overview.* www.dwavesys.com, Accessed: 2018-01-10. 3, 7, 8

[13] Trevor Lanting, AJ Przybysz, A Yu Smirnov, Federico M Spedalieri, Mohammad H Amin, Andrew J Berkley, R Harris, Fabio Altomare, Sergio Boixo, Paul Bunyk, et al. Entanglement in a quantum annealing processor. *Physical Review X*, 4(2):021041, 2014. 3

[14] Edward Farhi, Jeffrey Goldstone, Sam Gutmann, and Michael Sipser. Quantum computation by adiabatic evolution. *arXiv preprint quant-ph/0001106*, 2000. 4, 12

[15] C.C. McGeoch. *Adiabatic Quantum Computation and Quantum Annealing: Theory and Practice.* Synthesis Lectures on Quantum Computing. Morgan & Claypool Publishers, 2014. 4, 12, 14, 16

[16] N David Mermin. *Quantum computer science: an introduction.* Cambridge University Press, 2007. 4

[17] A. Yu. Kitaev, A. H. Shen, and M. N. Vyalyi. *Classical and Quantum Computation.* American Mathematical Society, Boston, MA, USA, 2002. 4

[18] Dorit Aharonov, Wim Van Dam, Julia Kempe, Zeph Landau, Seth Lloyd, and Oded Regev. Adiabatic quantum computation is equivalent to standard quantum computation. *SIAM review*, 50(4):755–787, 2008. 4, 12

[19] Brousentsov N. P., Maslov S. P., Ramil Alvarez J., and Zhogolev E.A. *Development of ternary computers at Moscow State University.* Russian Virtual Computer Museum. Accessed: 2018-01-07. 5

[20] Bas Hensen, Hannes Bernien, Anaïs E Dréau, Andreas Reiserer, Norbert Kalb, Machiel S Blok, Just Ruitenberg, Raymond FL Vermeulen, Raymond N Schouten, Carlos Abellán, et al. Loophole-free Bell inequality violation using electron spins separated by 1.3 kilometres. *Nature*, 526(7575):682–686, 2015. 7

[21] Zhi Zhao, Yu-Ao Chen, An-Ning Zhang, Tao Yang, Hans J Briegel, and Jian-Wei Pan. Experimental demonstration of five-photon entanglement and open-destination teleportation. *Nature*, 430(6995):54–58, 2004. 7

[22] E Hagley, X Maitre, G Nogues, C Wunderlich, M Brune, Jean-Michel Raimond, and Serge Haroche. Generation of Einstein-Podolsky-Rosen pairs of atoms. *Physical Review Letters*, 79(1):1, 1997. 7

[23] Markus Arndt, Olaf Nairz, Julian Vos-Andreae, Claudia Keller, Gerbrand Van der Zouw, and Anton Zeilinger. Wave–particle duality of C60 molecules. *nature*, 401(6754):680–682, 1999. 7

[24] Wikipedia, the free encyclopedia. *D-Wave Systems*. Accessed: 2018-01-10.
7

[25] D-Wave Systems Inc. *The D-Wave 2X^{TM} Quantum Computer Technology
Overview*. www.dwavesys.com, Accessed: 2018-01-10. 7

[26] Mark W Johnson, Mohammad HS Amin, Suzanne Gildert, Trevor Lant-
ing, Firas Hamze, Neil Dickson, R Harris, Andrew J Berkley, Jan Johans-
son, Paul Bunyk, et al. Quantum annealing with manufactured spins.
Nature, 473(7346):194–198, 2011. 8, 16

[27] M. Born and V. Fock. Beweis des Adiabatensatzes. *Zeitschrift für Physik*,
51(3):165–180, 1928. 10

[28] D.J. Griffiths. *Introduction to Quantum Mechanics*. Pearson international
edition. Pearson Prentice Hall, 2005. 10

[29] W. van Dam, M. Mosca, and U. Vazirani. How powerful is adiabatic quan-
tum computation? In *Proceedings 2001 IEEE International Conference
on Cluster Computing*, pages 279–287, Oct 2001. 13

[30] Kerson Huang. *Introduction to statistical physics*. CRC press, 2009. 16

[31] Sei Suzuki, Jun-ichi Inoue, and Bikas K Chakrabarti. *Quantum Ising
phases and transitions in transverse Ising models*, volume 862. Springer,
2012. 16

[32] T. Albash and D. A. Lidar. Evidence for a Limited Quantum Speedup on
a Quantum Annealer. *ArXiv e-prints*, May 2017. 16

[33] B. Gardas, J. Dziarmaga, and W. H. Zurek. Defects in Quantum Com-
puters. *ArXiv e-prints*, July 2017. 17, 18

[34] J. A. Bondy and U. S. R. Murty. *Graph Theory with Applications*. Elsevier,
New York, 1976. 24, 27

[35] G. Chartrand. *Introductory Graph Theory*. Dover Books on Mathematics
Series. Dover, 1977. 24, 27, 47

[36] N. Biggs. *Algebraic Graph Theory*. Cambridge Mathematical Library.
Cambridge University Press, 1993. 24, 47

[37] T. Krajewski, V. Rivasseau, and Zhituo Wang A. Tanasa. Topological
Graph Polynomials and Quantum Field Theory, Part I: Heat Kernel The-
ories. *J.Noncommut.Geom., LPT ORSAY 08-87*, 4:29–82, 2010. 24

[38] Otfried Gühne and Géza Tóth. Entanglement detection. *Physics Reports*,
474(1):1–75, 2009. 24

[39] Ueda, H., Takeuchi, T. T., and Itoh, M. A graph-theoretical approach for comparison of observational galaxy distributions with cosmological N-body simulations. *A&A*, 399(1):1–7, 2003. 24

[40] W.S. Massey. *A Basic Course in Algebraic Topology.* Graduate Texts in Mathematics. Springer New York, 1991. 26

[41] Andrew Lucas. Ising formulations of many NP problems. *Frontiers in Physics*, 2:5, 2014. 28, 29

[42] Di Wang and Robert Kleinberg. Analyzing quadratic unconstrained binary optimization problems via multicommodity flows. *Discrete Applied Mathematics*, 157(18):3746 – 3753, 2009. 28

[43] Worldatlas. *United Kingdom Outline Map.* www.worldatlas.com, Accessed: 2018-05-19. 30

[44] Cornelius Lanczos. An iteration method for the solution of the eigenvalue problem of linear differential and integral operators. *J. Res. Natl. Bur. Stand. B*, 45:255–282, 1950. 44

[45] Anders W. Sandvik. Computational Studies of Quantum Spin Systems. *AIP Conf.Proc.1297:135*, 2010. 44

[46] P. Prelovsek and J. Bonca. Ground state and finite temperature lanczos methods. *Strongly Correlated Systems Springer Series in Solid-State Sciences Volume 176, pp 1-30*, 2013. 44

[47] James Demmel, Jack Dongarra, Axel Ruhe, and Henk van der Vorst. *Templates for the Solution of Algebraic Eigenvalue Problems: A Practical Guide.* Society for Industrial and Applied Mathematics, Philadelphia, PA, USA, 2000. 44

[48] R. V. Mises and H. Pollaczek-Geiringer. Praktische Verfahren der Gleichungsauflösung . *ZAMM - Journal of Applied Mathematics and Mechanics / Zeitschrift für Angewandte Mathematik und Mechanik*, 9(2):152–164, 1929. 44

[49] J.P. Boyd. *Chebyshev and Fourier Spectral Methods: Second Revised Edition.* Dover Books on Mathematics. Dover Publications, 2001. 45

[50] Holger Fehske, Jens Schleede, Gerald Schubert, Gerhard Wellein, Vladimir S. Filinov, and Alan R. Bishop. Numerical approaches to time evolution of complex quantum systems. *Physics Letters A*, 373(25):2182 – 2188, 2009. 46

[51] Go. Torres-Vega. Chebyshev scheme for the propagation of quantum wave functions in phase space. *The Journal of Chemical Physics*, 99(3):1824–1827, 1993. 46

[52] Curt Wittig. The Landau-Zener Formula. *The Journal of Physical Chemistry B*, 109(17):8428–8430, 2005. PMID: 16851989. 48

[53] Le Tuan Anh Ho and Liviu F. Chibotaru. A simple derivation of the Landau-Zener formula. *Phys. Chem. Chem. Phys.*, 16:6942–6945, 2014. 48

[54] Clarence Zener. Non-adiabatic crossing of energy levels. *Proceedings of the Royal Society of London A: Mathematical, Physical and Engineering Sciences*, 137(833):696–702, 1932. 48

[55] L. Landau. Zur Theorie der Energieubertragung. II. *Physikalische Zeitschrift der Sowjetunion*, 2(46-51), 1932. 48

[56] Ryszard Rudnicki. *Wykłady z analizy matematyczej.* Wydawnictwo Naukowe PWN, 2006. 50